Improved color-gradient method for Lattice-Boltzmann modeling of two-phase flows

T. Lafarge [a),1,2] P. Boivin,[3] N. Odier,[1] and B. Cuenot[1]

[1)] *CERFACS, CFD Team, 42 Avenue G. Coriolis, Toulouse Cedex 01 31057, France*

[2)] *Safran Tech, Rue des Jeunes Bois – Châteaufort, 78772 Magny-Les-Hameaux, France*

[3)] *Aix Marseille Univ, CNRS, Centrale Marseille, M2P2, Marseille, France.*

(Dated: August 23, 2021)

This article presents a revised formulation of the color gradient method to model immiscible two-phase flows in the Lattice-Boltzmann framework. Thanks to this formulation, the Colour-Gradient method is generalised to *an arbitrary Equation of State under the form* $p = f(\rho, \phi)$, relieving the non-physical limitation between density and sound speed ratios present in the original formulation. A fourth-order operator for the equilibrium function is introduced, *and* its formulation is justified through the calculation of the 3rd order equivalent equation of this numerical scheme. A mathematical development demonstrating how the recoloration phase allows to solve a conservative Allen-Cahn equation is also proposed. Finally, a novel temporal correction is proposed, improving the numerical stability of the method at high density ratio. Validation tests up to density ratios of 1000 are presented.

[a)] *Author to whom correspondence should be addressed: thomas.lafarge@cerfacs.fr*

I. INTRODUCTION

The numerical simulation of interfacial multiphase flows constitutes a challenging subject of investigation in fluid mechanics. Those flows are defined by the co-existence of two immiscible phases. The transition between the two segregated phases is very sharp, and occurs over a few atoms length. For this reason, it is commonly assumed that the two phases are separated by an infinitely thin interface. An inter-molecular attractive forces imbalance occurs at this interface, resulting in surface tension, which has a significant impact on interface dynamics[1]. The interface leads to severe density gradients in the case of liquid-gas configurations, which is a challenge for numerical simulation. For atomization applications, the interface is also subject to intense shear, resulting in additional numerical difficulties. Furthermore, the interface curvature needs to be accurately estimated for an accurate pressure jump prediction, which is a challenge for complex flow topologies, such as interfacial waves, liquid ligaments, and associated break-up. Finally, atomization configurations involve large Reynolds and Weber numbers which results in a large range of scales[2].
Despite those difficulties, methodologies have been proposed to simulate such interfacial flows. On one hand, sharp interface methods consider separated phases with discontinuous quantities and jump conditions at the interface. The advection of a scalar quantity allows to track the interface. The Volume of Fluid (VoF)[3] method and the Level-Set methods[4] have allowed numerical predictions of realistic two-phase configurations, but suffer from a significant computational cost due to stark mesh resolution requirements in the interface. On the other hand, diffuse interface methods have also been proposed, in which the interface is considered as a smooth transition from one phase to the other. To allow such a continuous transition, the interface is artificially thickened over several grid points, which consequently reduces interfacial gradients and associated mesh constraints required for their discretization. Among these diffuse interface methods, the Phase Field Method has been first introduced, relying on the work of Van der Waals[5], Korteweg[6], Cahn and Hilliard[7]. Multifluid methods were later proposed by Baer and Nunziato[8], Saurel and Abgrall[9], Kapila[10], Saurel et *al.*[11,12]. Reviews for both phase-field and multi-fluid methods may be found in Anderson et *al.*[13] and Saurel and Pantano[14].

In the meantime, Lattice Boltzmann Method (LBM) has received a growing attention. Its basis have been originally proposed by the Cellular Automata community. Since Frish et

al.[15] and d'Humières et *al.*[16] who introduced the Lattice Gas Automata (LGA) Algorithm, Mc Namara and Zanetti[17] extended this work to propose a Lattice Boltzmann Method. Originally proposed for low-Mach aerodynamics, extensions to multi-phase flows rapidly came out. Rothman and Keller[18] proposed a LGA multiphase algorithm that has been adapted to a LBM framework by Gustensen et *al.*[19].

LBM received a growing interest motivated by its scalability and its low dissipation properties, making it particularly well-suited for acoustic long distance dispersion problems[20]. *It has been applied to a wide range of applications such as, reservoir permeability*[21–23]*, combustion flows*[24]*, blood flow*[25]*, boiling flow*[26]*, thermocapillarity flows*[27]*, non-Newtonian flows*[28]*, magneto-hydrodynamic flows*[29]*, cryogenic flows*[30]*, etc.* It also proved to be more computationally efficient than standard methods for aero-dynamics problems for example. Its application to two-phase *flows* have also largely been undertaken through the use of LBM, with several specific methodologies. Apart from the Colour Gradient Method[18] (also known as RK method from Rothman and Keller, their creator) Shan and Chen[31,32] proposed a Pseudo-potential method. Swift et *al.* introduced the Free Energy method[33,34] and He et *al.*[35] finally proposed the so-called HCZ method (from He, Chen and Zhang who first proposed the method), which recently received a lot of attention since the work of Fakhari[36–39] Geier et *al.*[40] and Mitchell[41]27. Having greatly benefited from the advances in the phase field community[42,43], these methods were applied on a large range of cases: droplet impact[44], free jet[45], ternary fluid[46], drop impact on a liquid film[47], flow with surfactant[48], direct-writing printing[49] and also widely in porous flow[50]. HCZ method allows to simulate a large range of flows at both large density ratios and large Reynolds numbers[41], while other methods are limited to moderate density ratios and / or moderate Reynolds numbers.

Despite the attractiveness of this last method, it takes place in an incompressible framework. The need to account for compressibility is of importance for several two-phase configurations. A typical application of the present work is liquid injection, where cavitation occurs[51] and atomization may be impacted by acoustics[52–57]. For such problems, other methods than HCZ must then be investigated.

Despite the complexity of obtaining equivalent macroscopic equations[58–60], we decided here to revisit the color gradient method, for its simplicity and numerical efficiency[61]. *In the present work, a reformulation of the method is proposed. This new formulation is mathematically equivalent to the classical one, but is numerically more efficient*. In particular,

it is adapted to an arbitrary Equation Of State (EOS), and a new physical interpretation of the method is proposed. Using another approach than the one proposed by Subhedar[60], the equivalent macroscopic equation associated with the recoloration step of the algorithm – accounting for phase segregation – is proposed. It is shown that the recoloration step allows to solve an advection-diffusion equation. Finally those analyses highlight a temporal spurious term, which can be corrected by a new correction term, which significantly improves numerical stability, thus allowing to tackle density ratios as high as 1000.

This paper is organized as follows: governing equations and the considered isothermal thermodynamic closure are presented in section II. The original Color-Gradient algorithm is recalled in III, in which our revised Color-Gradient algorithm is also presented. Section IV proposes novel physical insights for the proposed algorithm. Relation between spurious currents and isotropy conditions are discussed, a physical interpretation for the recoloration step is provided, and accurate corrections to predict a sheared interface are detailed. Finally, results are provided in section V and conclusions are drawn in section VI.

II. TWO-PHASE FLOW GOVERNING EQUATIONS

Isothermal two-phase flows with density gradient and sheared interface are described with the governing equations and thermodynamic closure detailed in this section.

A. Conservation equations

Mass and momentum conservation equations read

$$\partial_t \rho + \partial_\alpha \rho u_\alpha = 0\,, \tag{1}$$

$$\partial_t \rho u_\alpha + \partial_\beta \left(\rho u_\alpha u_\beta + \delta_{\alpha\beta} p + p^\sigma_{\alpha\beta} - \mathcal{T}_{\alpha\beta}\right) = F_\alpha\,, \tag{2}$$

where α and β denote spatial directions, ∂_α and ∂_β the partial derivative in α and β directions, ρ the two phases's density, u_α the velocity, p the thermodynamic pressure, $\delta_{\alpha\beta}$ the Kronecker function, $p^\sigma_{\alpha\beta}$ a pressure tensor representing surface tension, $\mathcal{T}_{\alpha\beta}$ the stress tensor and F_α being a volumic force. It must be noted that the Einstein's summation formalism is used in this work. The stress tensor reads:

$$\mathcal{T}_{\alpha\beta} = \rho\nu\left(\partial_\beta u_\alpha + \partial_\alpha u_\beta\right) + \rho(\nu_b - \nu)\frac{2}{D}\left(\partial_\gamma u_\gamma\right)\delta_{\alpha\beta}, \tag{3}$$

ν being the kinetic shear viscosity, ν_b the kinetic bulk viscosity and D the spatial dimension of the system. Once the total density is known, the knowledge of the composition is required to close the system. Several field can be calculated in order to close the system, such as one of the phase's density (ρ_k stands for the k^{th} phase density), the density ratio of the k^{th} phase, noted Y_k or any field useful to discriminate the two phases. In this work, the additional conservation equation is accounted for through the conservation of a phase field parameter ϕ defined as

$$\phi = \frac{\rho_1 - \rho_2}{\rho} = Y_1 - Y_2, \tag{4}$$

By definition, this equation is equal to 1 when located in a pure phase 1 environment and to -1 in a pure phase 2 environment. The equation for the phase field parameter ϕ is defined in Sec. IV B.

The presence of one single momentum equation Eq. (2) implies a mechanical equilibrium assumption: the two phases are assumed to be in velocity and pressure equilibrium:

$$\begin{cases} u_1 = u_2 \\ p_1 = p_2 \end{cases} \tag{5}$$

The surface tension term $p^{\sigma}_{\alpha\beta}$ was proposed by Gueyffier and Zaleski[62] *and introduced in the LBM framework by Reis and Phillips*[58]*. It is given by:*

$$p^{\sigma}_{\alpha\beta} = \sigma[\delta_{\alpha\beta - n_\alpha n_\beta}]\delta_{interface} \tag{6}$$

with $\vec{n}$ being an estimation of the normal to the interface, and $\delta_{interface}$ is a function that allows to locate the interface. They are given by:

$$n_\alpha = \frac{\partial_\alpha \phi}{|\vec{\nabla}\phi|} \qquad \delta_{interface} = \frac{|\vec{\nabla}\phi|}{2} \tag{7}$$

Note that the phase field used to solve the system, and the phase field used to calculate the surface tension term don't have to be the same. It is notably the case in the work of Saurel and Perigaud[63] *who uses the volume fraction or in the work of Ba et al.*[64] *that uses a modified version of ϕ. To the authors knowledge, the impact of the used phase field on the capability to predict surface tension haven't been investigated. For the sake of simplicity, the same phase field ϕ is then used for the surface tension operator and for solving the composition of the density.* In this model, surface tension is modeled as a pressure tensor (see Eq. (2)).

The fact that surface tension could take the form of stress tensor was first demonstrated by Korteweg[6], and the current model, referred to as CSS (Continuous Surface Stress), was proposed by Gueyffier and Zaleski[62]. It relies on the same geometrical background as the CSF (Continuous Surface Force) model proposed by Brackbill et al.[65], i.e. both of them are equivalent to a volumic force proportional to an estimation of the curvature.

B. Thermodynamic closure

To close the above system, a thermodynamic closure is required, which can be written generically as:

$$p = f(\rho, Y_1) = g(\rho, \phi). \tag{8}$$

Note that the equation of state (EOS) necessarily differs from $p = \rho c_s^2$ (c_s being the speed of sound), classically used in athermal Lattice-Boltzmann modelling[66]. In the classical color gradient formulation[67], the closure relation reads:

$$p = \rho Y_1 c_1^2 + \rho Y_2 c_2^2, \tag{9}$$

with c_1 and c_2 are the speed of sound in each phase, chosen to ensure mechanical equilibrium. This equation of state proposed by Grunau et al.[68] presents a major drawback for high density ratios, as it implies

$$\frac{c_2^2}{c_1^2} = \frac{\rho_1}{\rho_2}. \tag{10}$$

This drawback can easily be illustrated considering the liquid-air system: for a density ratio of 1000, the air sound speed $c_{s,2} = 347 m.s^{-1}$ would imply a liquid sound speed of $c_{s,2} = 11 m.s^{-1}$. In such conditions, any liquid flow speed above $3 m.s^{-1}$ would correspond to a local Mach number over 0.3, and therefore create non-physical compressible effects.

To circumvent this limitation, an Equation Of State (EOS) is used, inspired from the Stiffened Gas formulation[69] $p = \rho(c_p - c_v).T - p_\infty$ for each phase, where p_∞ accounts for the attractive forces in the liquid. Assuming an isothermal fluid, the equation of state in each phase k only differs from the classical athermal EOS used in LBM by $p_{\infty,k}$, as:

$$p_k = \rho_k c_k^2 - p_{\infty,k}. \tag{11}$$

Note that $p_{\infty,k}$, c_k are constants of the flows. Finally, a mixture equation of state for the

two-phase flow by assuming mechanical equilibrium[51,70], is derived:

$$p = p_k, \forall k, \tag{12}$$

yielding

$$\frac{1}{\rho} = \frac{Y_1}{\rho_1} + \frac{Y_2}{\rho_2} = \frac{Y_1 c_1^2}{p + p_{\infty,1}} + \frac{Y_2 c_2^2}{p + p_{\infty,2}}, \tag{13}$$

which can be inverted to provide explicitly the expression required in Eq. (8), e.g.

$$p = \frac{1}{2}\left(\rho\hat{c}^2 - p_{\infty,1} - p_{\infty,2} + \sqrt{\left(p_{\infty,2} - p_{\infty,1} + \rho\bar{c}^2\right)^2 + \rho^2(1-\phi^2)c_1^2 c_2^2}\right) \tag{14}$$

where $\hat{c}^2 = \frac{c_1^2+c_2^2}{2} + \phi\frac{c_1^2-c_2^2}{2}$ and $\bar{c}^2 = \frac{c_1^2-c_2^2}{2} + \phi\frac{c_1^2+c_2^2}{2}$. *Derivation of Eqs. (13, 14) and proof of the pressure's positivity can be found in the literature*[71] *in the more general non-isothermal case.*

Note nonetheless that the present work is compatible with any other EOS which can be written under the generic form Eq. (8).

III. LATTICE-BOLTZMANN MODEL

For the sake of simplicity, the presentation of the Lattice-Boltzmann model is performed in 2D, based on the classical D2Q9 nearest-neighbor lattice[66]. Discrete velocities are introduced as:

$$\vec{\xi}_i = \frac{\Delta x}{\Delta t}\begin{cases} (0,0) & i = 0 \\ (\pm 1, 0) \ or \ (0, \pm 1) & i = 1,3,5,7 \\ (\pm 1, \pm 1) \ or \ (\pm 1, \mp 1) & i = 2,4,6,8 \end{cases}, \tag{15}$$

where Δx and Δt are respectively the space and time discretization. To each discrete velocity is assigned a weight[66] ω_i (lattice-dependent). A characteristic lattice velocity c_s, related to the speed of sound[66], is defined as:

$$c_s = \frac{\Delta x}{\sqrt{3}\Delta t}. \tag{16}$$

A. Color gradient method

The color-gradient method is the first Lattice Boltzmann method introduced for two-phase flows. Initially derived in the Lattice Gas Automata framework[18], it has been successively transported to a LBM framework by Gustensen[19], the current recoloration operator was proposed by Latva-Kokko[72], the surface tension operator by Reis and Phillips[58],

and successive improvements and generalization to more than 2 species were proposed by Leclaire[67,73–75]. The fluid is represented by two probability density functions $(f_i^{(1)}, f_i^{(2)})$ related to each fluid mass volume (ρ_1, ρ_2) as

$$\rho_k = \sum_i f_i^{(k)}. \tag{17}$$

It should be underlined, that this formalism is only proposed for discrete density functions, to the author knowledge, it cannot be transposed to continuous equations. For this model, mechanical equilibrium is assumed (Eqs. (5)), and the mixture's momentum reads

$$\rho u_\alpha = \sum_i \sum_k \xi_{\alpha,i} f_i^{(k)} \tag{18}$$

Each population $(f_i^{(1)}, f_i^{(2)})$ is calculated via a three-step algorithm:

Step 1: collision is achieved via

$$f_i^{(k),*} = f_i^{(k)} + \Omega_i^{(1),k} + \Omega_i^{(2),k}, \tag{19}$$

where $\Omega_i^{(1),k}$ is the collision operator, relaxing the population towards the Maxwell-Boltzmann equilibrium distribution function $f_i^{(k,eq)}$. For the BGK (Bhatnagar-Gross-Krook) single relaxation time model[76], the collision term reads

$$\Omega_i^{(1),k} = -\frac{1}{\tau}\left(f_i^{(k)} - f_i^{(k,eq)}\right), \tag{20}$$

where the dimensionless relaxation time τ is related to the fluid viscosity through

$$\tau = \frac{\nu}{\Delta t c_s^2} + \frac{1}{2} \tag{21}$$

In Eq. (19), $\Omega_i^{(2),k}$ is a second collision term which accounts for surface tension, further detailed in Eq. (45).

Step 2: recoloration. The recoloration step – giving its name to the method – is applied to the total population $f_i = f_i^{(1)} + f_i^{(2)}$, taking the form

$$f_i^{(k),**} = Y_k f_i^* \pm \Omega_i^{(3)} \tag{22}$$

where Y_k is the mass fraction of the k^{th} phase, and $\Omega_i^{(3)}$ is a third collision function accounting for the fluid segregation.

Step 3: streaming. Finally, each population is streamed, accounting for the convective part of the macroscopic equations[66]:

$$f_i^{(k)}(x + \xi_i \Delta t, t + \Delta t) = f_i^{(k),**}(x, t). \tag{23}$$

In this formulation, the first two steps (collision and recoloration) are executed twice: once per population. Moreover, two equilibrium functions ($f_i^{(1,eq)}, f_i^{(2,eq)}$) have to be computed. In practice, the same collision model is applied to both phase and the model can be recast as follows, thereby limiting the number of operations per time-step.

B. Revised color-gradient algorithm

To minimize the number of operations per time step, let us consider

$$f_i = f_i^{(1)} + f_i^{(2)}, \tag{24}$$

corresponding to the total density $\rho = \rho_1 + \rho_2$, and

$$g_i = f_i^{(1)} - f_i^{(2)}, \tag{25}$$

related to the phase field function ϕ defined in Eq. (4) through

$$\rho\phi = \sum_i g_i. \tag{26}$$

The three steps described in Sec. III A can then be expressed as follows.

Step 1: collision. is recast as:

$$f_i^* = f_i^{eq} + \Omega_i^{(1)} + \Omega_i^{(2)} + \frac{1}{2} S_i, \tag{27}$$

where $\Omega_i^{(1)}$ is the collision operator, detailed in Eq. (20), $\Omega_i^{(2)}$ is the surface tension operator which will be detailled later (Eq. (45)), and S_i is a forcing term, also detailed later (Eq. (51)).

Step 2: recoloration.

The recoloration step writes now:

$$g_i^* = \phi f_i^* + \Omega_i^{(3)} \tag{28}$$

with $\Omega_i^{(3)}$the collision operator accounting for phase segregation, further detailed in Eq(48).

Step 3: streaming. Both f_i and g_i populations are then streamed, through

$$f_i(x + \xi_{\alpha,i}\Delta t, t + \Delta t) = f_i^*(x, t) \tag{29}$$

$$g_i(x + \xi_{\alpha,i}\Delta t, t + \Delta t) = g_i^*(x, t) \tag{30}$$

In the subsequent subsections, the proposed equilibrium function, the collision terms, and the force term S_i for the revised color gradient method are given.

C. Equilibrium part

The equilibrium function considered here reads:

$$f_i^{eq} = \rho w_i \left(H_{0,i} + u_\alpha \frac{H_{\alpha,i}}{c_s^2} + u_\alpha u_\beta \frac{H_{\alpha\beta,i}}{2c_s^4} \right) + (p - \rho c_s^2) \left(E_i + u_\alpha \frac{w_i H_{\beta\beta\alpha,i}}{2c_s^6} \right), \tag{31}$$

where the first terms correspond to the classical formulation[66], and the last one allows to consider an arbitrary EOS (e.g. when $p \neq \rho c_s^2$). In Eq. (31), $H_{\alpha,i}$ are the Hermite polynomials, provided in Appendix A. In this work, the moment m_* associated to the Hermite polynomial H_* is defined by

$$m_* = \sum_i H_{*,i} f_i. \tag{32}$$

Similarly, the moment of the equilibrium function associated with the Hermite polynomial H_* is noted m_*^{eq}. The equilibrium function of (Eq. (31)), is designed so that its low-order moments follow:

$$m_0^{eq} = \rho \tag{33}$$

$$m_\alpha^{eq} = \rho u_\alpha \tag{34}$$

The second-order moment is obtained by pointing out that the macroscopic equation corresponding to the equilibrium part follows[77]:

$$\partial_t m_\alpha^{eq} + \partial_\beta \left(m_{\alpha\beta}^{eq} + m_0 c_s^2 \delta_{\alpha\beta} \right) = F_\alpha + O(\Delta t), \tag{35}$$

corresponding to the Eulerian part of the momentum equation Eq. (2):

$$\partial_t \rho u_\alpha + \partial_\beta \left(\rho u_\alpha u_\beta + p\delta_{\alpha\beta} \right) \delta_{\alpha\beta} = 0. \tag{36}$$

Comparing the two previous equations, the second order moment of the equilibrium has to be:

$$m^{eq}_{\alpha\beta} = \rho u_\alpha u_\beta + (p - \rho c_s^2)\delta_{\alpha\beta} \tag{37}$$

The definition of the third moment depends on the considered numerical scheme. In a Lattice Boltzmann framework, the number of discrete velocities is directly related to the number of moments that are recovered correctly[66]. For instance, not all three order moments (i.e. the moments linked to the third degree Hermite's polynomial: H_{xxx}, H_{xxy}, H_{xyy} and H_{yyy} in D2Q9) can be correctly recovered[66]: $\sum_i w_i H_{xxx,i} f_i^{eq} = \sum_i w_i H_{yyy,i} f_i^{eq} = 0$ for all f_i^{eq}. The consequence is that, while the third moments of f_i^{eq} should be

$$m^{eq}_{\alpha\beta\gamma} = (p - \rho c_s^2)(u_\alpha \delta_{\beta\gamma} + u_\beta \delta_{\alpha\gamma} + u_\gamma \delta_{\alpha\beta}), \tag{38}$$

it actually reads:

$$\begin{cases} m^{eq}_{\alpha\alpha\beta} = (p - \rho c_s^2) u_\beta & \alpha \neq \beta \\ m^{eq}_{\alpha\alpha\alpha} = 0 & otherwise \end{cases} \tag{39}$$

This problem has already been discussed by Wen et al.[78], and the proposed solution is to adopt the forcing strategy proposed by Li et al.[79] for the color-gradient framework, leading to the forcing term S_{Sp} given in Eq. (53).

In the equilibrium distribution function Eq.(31), a new isotropic operator E_i is introduced as:

$$E_i = w_i \left(\frac{H_{xx,i} + H_{yy,i}}{2c_s^4} - \frac{H_{xxyy}}{4c_s^6} \right). \tag{40}$$

The derivation and discussion of this operator is addressed in Sec. IV A.

Note that for the $D2Q9$ lattice[66], $E_i = \frac{w_i - \delta_{i,0}}{c_s^2}$, showing that this formalism reduces to the following, classically found in the literature[80,81] despite being more related to the free-energy community:

$$\begin{cases} f_i^{eq} = w_i \left(\frac{p}{c_s^2} + \rho \left(u_\alpha \frac{H_{\alpha,i}}{c_s^2} + u_\alpha u_\beta \frac{H_{\alpha,i}}{2c_s^4} \right) \right) + (p - \rho c_s^2) u_\alpha \frac{H_{\beta\beta\alpha}}{2c_s^6} & i = 1..8 \\ f_0^{eq} = \rho - \sum_{1..8} f_i^{eq} \end{cases} \tag{41}$$

D. Collision step: $\Omega_i^{(1)}$

In LB methods, the collision term $\Omega_i^{(1)}$ (Eq. (19)) relaxes the population towards the so-called equilibrium distribution function Eq. (31).

In practice, the BGK collision operator[76] is quite limited in terms of stability[82]. To enhance stability, a regularized collision operator[82] is used in this study. The effect of the bulk viscosity is also accounted for following the method by Renard et al[83].

The proposed collision term reads

$$\Omega_i^{(1)} = \left(1 - \frac{1}{\tau_\nu}\right)\left(f_{xy,i}^{r,neq} + f_{\nu,i}^{r,neq}\right) + \left(1 - \frac{1}{\tau_b}\right) f_{b,i}^{r,neq} \tag{42}$$

where $f_{\nu,i}^{r,neq}$ and $f_{b,i}^{r,neq}$ are the projections of the non-equilibrium counterpart of the population function on respectively the H_ν and H_b polynomials:

$$f_{k,i}^{r,neq} = \frac{H_{k,i}}{c_s^4} \sum_i \left(f_i - f_i^{eq} + \frac{1}{2} S_i\right) H_{k,i}, \quad k = \nu, b, xy. \tag{43}$$

where S_i is a source term detailled afterward that introduces volumic forces, surface tension and correction terms. The dimensionless relaxation times (τ_ν, τ_b) depend on the kinematic viscosity ν and bulk viscosity ν_b as:

$$\tau_\nu = \frac{p\nu}{\rho \Delta t} + \frac{1}{2} \qquad \tau_b = \frac{p\nu_b}{\rho \Delta t} + \frac{1}{2} \tag{44}$$

E. Collision step: $\Omega_i^{(2)}$

The collision term $\Omega_i^{(2)}$ introduces surface tension to the model:

$$\Omega_i^{(2)} = \frac{\sigma w_i}{4|\vec{C}|c_s^4} \left(\frac{\left(2C_x C_y H_{xy,i} + (C_x^2 - C_y^2) H_{\nu,i}\right)}{\tau_\nu} - \frac{(C_x^2 + C_y^2) H_{b,i}}{\tau_b} \right) \tag{45}$$

This operator is a reformulation of the one proposed by Liu et al.[59], taking into account the different relaxation times for the moments of H_ν and H_b. $\vec{C}$ refers to the colour gradient that gave the method's name and σ is the surface tension $(kg.s^{-2})$. The colour gradient can be seen as an approximation of the spatial gradient of the phase field as showed by Leclaire et al.[67]. Among the discretization scheme proposed in[67], we chose the one providing the highest level of isotropy while involving the first neighbours only:

$$C_\alpha(x,t) = \sum_i \frac{w_i \xi_{\alpha,i} \phi(x + \xi_{\alpha,i}\Delta t, t)}{c_s^2} = \Delta t \partial_\alpha \phi + O(\Delta t^2) \tag{46}$$

When $\tau_\nu = \tau_b = \tau$, this formulation is equivalent to the one proposed by Reis & Phillips[58]. where the operator $\Omega_i^{(2)}$ is designed in order to guarantee

$$\sum_i \xi_{\alpha,i} \xi_{\beta,i} \Omega_i^{(2)} = \frac{p_{\alpha\beta}^\sigma}{\tau} \tag{47}$$

with $p_{\alpha\beta}^\sigma$ the pressure tensor introducing surface tension described in II

F. Recoloration step: $\Omega_i^{(3)}$

The recoloration step applies to the phase-field population g_i (Eq. (28)) and reads

$$\Omega_i^{(3)} = w_i \frac{p(1-\phi^2)}{2W} \frac{\xi_{\alpha,i}\partial_\alpha \phi}{c_s^2 |\vec{\nabla}\phi|} \tag{48}$$

where W has the dimension of a length (m) and corresponds to the characteristic width of the interface (see Sec. IV B). This term was originally proposed by Latva-Kokko[72] inspired by the work of D'Ortona[84] and later improved by Halliday et *al.*[85]. The present formalism is strictly equivalent to the one proposed by Halliday et *al.*[85], where the source term[85] is given by:

$$\Omega_i^{(3),Hal} = \beta \frac{\rho_1 \rho_2}{\rho^2} f_i^{eq}(u=0) \frac{\partial_\alpha \phi}{|\vec{\nabla}\phi|} \xi_{\alpha,i} \tag{49}$$

with β a constant, $f_i^{eq}(u=0)$ the equilibrium function given in (31) *with all the velocity terms equal to zero. Taking into consideration the fact that $E_i = \frac{w_i - \delta_{i,0}}{c_s^2}$, then $f_i^{eq}(u = 0)\xi_{\alpha,i} = w_i \frac{p\xi_{\alpha,i}}{c_s^2}$. By definition of ϕ, it can be shown that: $\frac{\rho_1\rho_2}{\rho^2} = \frac{1-\phi^2}{4}$, then Halliday's term reduces to:*

$$\Omega_i^{(3),Hal} = \beta w_i \frac{p(1-\phi^2)}{4} \frac{\xi_{\alpha,i}\partial_\alpha \phi}{c_s^2 |\vec{\nabla}\phi|} \tag{50}$$

Then it comes that both formulations are equivalent for $\beta = \frac{2}{W}$.

G. Forcing term S_i

In this work, the forcing term consists of three contributions

$$S_i = S_{F,i} + S_{Sp,i} + S_{t,i}. \tag{51}$$

S_F is a source term accounting for potential volume forces, e.g. gravity. Given a force F_α,

$$S_{F,i} = w_i \left(F_\alpha \frac{H_{\alpha,i}}{c_s^2} + (u_\alpha F_\beta + u_\beta F_\alpha) \frac{H_{\alpha\beta,i}}{2c_s^4} \right). \tag{52}$$

S_{Sp} is a corrective term which corrects the error stemming from the third order moment, improperly resolved on the D2Q9 lattice[78,79,86]:

$$S_{Sp,i} = w_i \left(3 \frac{\partial_y[(p-\rho c_s^2)u_y] - \partial_x[(p-\rho c_s^2)u_x]}{2c_s^4} H_{\nu,i} - \frac{\partial_y[(p-\rho c_s^2)u_y] + \partial_x[(p-\rho c_s^2)u_x]}{2c_s^4} H_{b,i} \right) \tag{53}$$

This expression corresponds to the correction introduced by Wen et al.[78] recast in the present formalism. The derivative terms are calculated with the scheme proposed in Eq. (46).

Finally, a novel temporal correction term is proposed in this work:

$$S_{t,i} = \left[p(x,t) - p(x,t-\Delta t) + (\rho(x,t) - \rho(x,t-\Delta t))c_s^2\right] E_i. \tag{54}$$

The derivation of Eqs. (53, 54) is provided in Sec. IV C.

H. Units and dimension

All values in the present paper are physical units, even though dimensionless Lattice-Boltzmann units are manipulated in the algorithm[66]. Physical and Lattice-Boltzmann units are linked through a characteristic density (ρ_{ref}), a characteristic speed and a characteristic length. The authors followed the common practice[66] in LBM to set the spatial step Δx as characteristic length, and the ratio $\frac{\Delta x}{\Delta t}$ as characteristic velocity (i.e. $c_s = 1/\sqrt{3}$ in Lattice Boltzmann Units (l.b.u.)). The characteristic density is chosen so that the heaviest fluid density is unity.

IV. ALGORITHM JUSTIFICATION AND DISCUSSION

A. Isotropic operator for arbitrary equation of state

The choice of operator E_i is of paramount importance to regulate spurious current[80].

In order to satisfy the moments of the equilibrium function given in Eqs. (33, 34, 37), E_i must only have non-zero second order moments in *Hermite* polynomial. :

$$\sum_i H_{\alpha\beta,i} E_i = 0 \tag{55}$$

$$\sum_i H_{x,i} E_i = \sum_i H_{y,i} E_i = \sum_i H_{xy,i} E_i = 0 \tag{56}$$

$$\sum_i H_{xx,i} E_i = \sum_i H_{yy,i} E_i = 1 \tag{57}$$

$$\sum_i H_{xxy,i} E_i = \sum_i H_{yyx,i} E_i = 0 \tag{58}$$

For the sake of simplicity, let us assume $\tau_\nu = \tau_b$ in the remainder of this section.

At this point, our system has only 8 moments for 9 unknownsns weights. It can be completed by the moment of H_{xxyy}. This moment must be chosen wisely and a random choice can lead to highly unstable behaviour, even for simple case at low density ratio. H_{xxyy} being a high degree polynomial, its impact on the macroscopic equation cannot be determined using the Chapmann-Enskog development, but can be found via a Taylor expansion[77,87].

The complete expansion, summarized in Appendix B indicates that the moments of the equilibrium functions are solution of the following equation:

$$\partial_t m^{eq}_\alpha + \partial_\beta \left(m^{eq}_{\alpha\beta} + m_0 c_s^2 \delta_{\alpha\beta} \right) = \mathcal{T}_{\alpha\beta} + \Delta t^2 \partial_\beta (O(\partial_t \mathcal{T}_{\alpha\beta}) + O(\partial_\gamma \Pi^{(1)}_{\alpha\beta}) + O(\Delta t^3) \tag{59}$$

with $\Pi^{(1)}_{\alpha\beta}$ the third moment of the non-equilibrium function. Its formulation is given by:

$$\Pi^{(1)}_{\alpha\beta\gamma} = \partial_t m^{eq}_{\alpha\beta\gamma} + \partial_\mu \left(m^{eq}_{\alpha\beta\gamma\mu} + \left[m^{eq}_{\alpha\beta} \delta_{\gamma\mu} + m^{eq}_{\beta\gamma} \delta_{\alpha\mu} + m^{eq}_{\alpha\gamma} \delta_{\beta\mu} \right] c_s^2 \right) \tag{60}$$

It comes that the Δt^2 error induced by the scheme has two components, one proportional to the time derivative of the stress tensor, and one proportional to $\Pi^{(1)}_{\alpha\beta}$. It is expressed as a function of the moments of the equilibrium function and the equilibrium function can be decomposed as follow: $f_i^{eq} = f_i^0 + (p - \rho c_s^2) E_i$, then all the moments of f_i^{eq} can also be decomposed in the same manner: $m_*^{eq} = m_*^O + \sum_i H_* E_i (p - \rho c_s^2)$ From this last decomposition, if note Er the component of $\Pi^{(1)}_{\alpha\beta\gamma}$ coming from the E_i counterpart of the equilibrium function, it comes:

$$\begin{aligned} Er = \partial_t \sum_i H_{\alpha\beta\gamma,i} E_i (p - \rho c_s^2) + \\ \partial_\mu \left[\left(\sum_i H_{\alpha\beta\gamma\mu,i} E_i + \sum_i \left[H_{\alpha\beta,i} \delta_{\gamma\mu} + H_{\beta\gamma,i} \delta_{\alpha\mu} + H_{\alpha\gamma,i} \delta_{\beta\mu} \right] c_s^2 E_i (p - \rho c_s^2) \right) \right] \end{aligned} \tag{61}$$

Using Eqs. (57 58), the expression of the error can be simplified. It comes than the error term can be cancelled when:

$$\sum_i H_{\alpha\beta\gamma\mu,i} E_i = - \left(\delta_{\alpha\beta} \delta_{\gamma\mu} + \delta_{\beta\gamma} \delta_{\alpha\mu} + \delta_{\alpha\gamma} \delta_{\beta\mu} \right) c_s^2 \tag{62}$$

or, equivalently on the D2Q9 lattice

$$\sum_i H_{xxyy,i} E_i = -c_s^2 \tag{63}$$

The system being closed, we finally have the formula given earlier (40):

$$E_i = w_i \left(\frac{H_{xx,i} + H_{yy,i}}{2c_s^4} - \frac{H_{xxyy}}{4c_s^6} \right) \tag{64}$$

The condition proposed in Eq. (62) happens to also be an isotropic condition as already discussed by Burgin[88]. A more general discussion about isotropy is proposed by Suiker[89], and the issue was largely tackled at the time of Lattice Gas Automata by Wolfram[90]. Subhedar[60] also discussed the importance of isotropy for the recoloration operator.

Illustration

The efficiency of this isotropic formulation Eq. (63) can be evaluated through the testcase of a static droplet. In a squared box with periodical boundary conditions, a spherical droplet of density $\rho_1 = 10kg.m^{-3}$ is set into an atmosphere of a lower densityt fluid ($\rho_2 = 1kg.m^{-3}$). The surface tension is set to 0, and the velocity field is initiated at 0 in all the domain. Giving the absence of phenomena able to animate the fluids, the flow is supposed to stay still, which makes it ideal to observe the spurious currents induced by the numerical scheme. The other parameters of the case are given afterward. The space step is $\Delta x = 0.001m$, the number of points in the x and y directions are $N_x = N_y = 128$ and the time step is $\Delta t = 1,6638.10^{-6}s$. The radius of the droplet is a multiple of the grid size: $R = 20\Delta x$ and so does the width of the interface $W = 2\Delta x$ (as a reminder, W is the parameter of the collision term in the recoloration operation Eq(48)). The shear viscosity of the fluids are set equal, and the bulk viscosity is equal to the shear viscosity: $\nu_1 = \nu_2 = \nu_{b,1} = \nu_{b,2} = 0.001m^2.s^{-1}$. The parameters of the equation of states (Eq. (11)) are $c_1 = c_2 = 347m.s^{-1}$, $p_{\infty,2} = 0$ and $p_{\infty,1}$ is set in order to ensure mechanical equilibrium $p_1 = p_2 = 120409Pa$.

Two cases are compared, one with E_i defined with $\sum_i H_{xxyy}E_i = 0$, and a second one satisfying the isotropic condition given in Eq. (63). In Fig. 1, the spurious currents induced by the two methods are compared after 2000 iterations. The location of the interface is given by the line $\phi = 0$, and the velocity field is represented with arrows, whose length has a scale of $1m.s^{-1}$. In the non-isotropic case, it can be seen that strong spurious currents appear in the interface, reaching a maximum value of velocity of $53m.s^{-1}$. These spurious currents are strong enough to deform the interface shape. Around 4000 iterations, numerical instabilities led to the failure of the computation. In the isotropic case, the spurious currents

are not visible (the maximum value of spurious velocity is $1.210^{-3} m.s^{-1}$), and the initial shape of the droplet is preserved. This illustrates the capability of this isotropic operator to reduce drastically the spurious currents. Note that the value for the non-isotropic operator $\sum_i H_{xxyy} E_i = 0$ has been chosen arbitrarily, and similar results can be obtained for other values different from $-c_s^2$

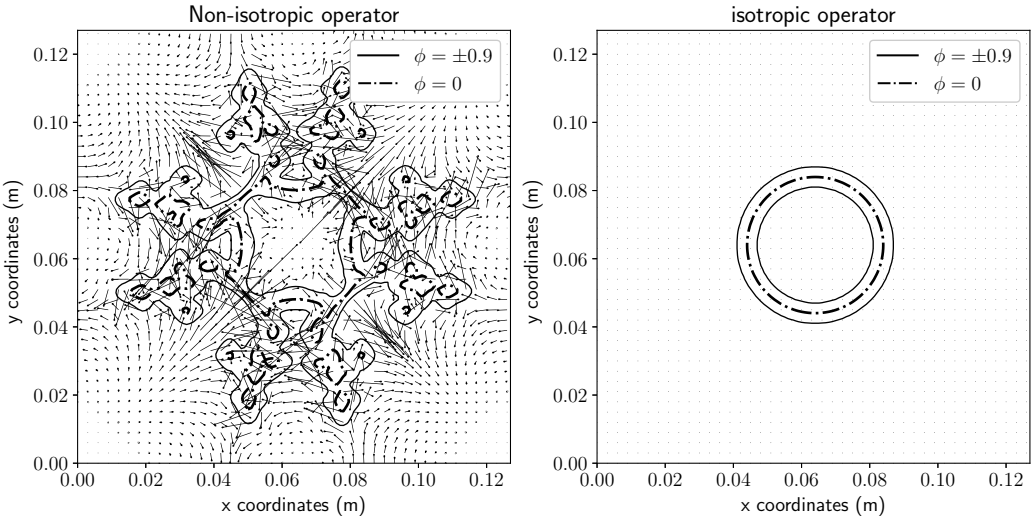

Figure 1: Case of a static bubble in a quiescent atmosphere with two different operators,one without the isotropic condition, i.e. $\sum_i H_{xxyy,i} = O$ (left), and one with it (right). The interface is represented by the $\phi = 0$ isolines and the velocity field by arrows of length scaled by $1 m.s^{-1}$

B. Recoloration and capillary effects

Through a Taylor expansion inspired by Dubois[87] (Appendix D), the macroscopic equation solved by the phase field calculated through the recoloration algorithm is obtained as:

$$\partial_t \rho\phi + \partial_\alpha(\rho\phi u_\alpha) = \partial_\alpha \left[\frac{p\Delta t}{2} \left(\partial_\alpha \phi - \frac{1-\phi^2}{W} n_\alpha \right) \right] + O(\Delta t^2), \tag{65}$$

The left side of the above equation is the Eulerian derivative, the right side related to the interface is itself composed of two terms, one diffusive term: $\partial_\alpha \frac{p\Delta t}{2}$ and one anti-diffusive term: $\partial_\alpha \phi$ and one $\partial_\alpha \left(\frac{p\Delta t}{2} \frac{1-\phi^2}{W} n_\alpha \right)$. The two effects are antagonist and they enventually

compensate each other, meaning that the width of the interface can be controlled. Actually, in the case of a steady flat interface in a quiescent flow, it can be shown that the interface stabilizes in a hyperbolic tangent profile:

$$\phi = \tanh\left(\frac{x - x_\epsilon}{W}\right) \tag{66}$$

with x_ϵ the location of the interface $\phi = 0$. Since $tanh(2.65) \approx 0.99$ the terminal thickness of the interface can be approximated at $5W$. It is interesting to notice that the anti-diffusion force is simulated through the third collision term $\Omega^{(3)}$, while the diffusive term is induced by the recoloration step. It shows that the recoloration scheme allows to solve an advection-diffusion type equation in a LBM framework in an efficient way. A drawback of this method is that the diffusion rate (i.e., the $\frac{p\Delta t}{2}$ factor) is implied by the numerical scheme and then cannot be set freely. It is interesting to compare the current equation (65) to the conservative Allen-Cahn equation proposed by Chiu & Lin[43] expressed by:

$$\partial_t \phi + \partial_\alpha(\phi u_\alpha) = \partial_\alpha\left[M\left(\partial_\alpha \phi - \frac{1-\phi^2}{W} n_\alpha\right)\right] \tag{67}$$

M being a constant named the mobility factor which has the dimension of a diffusion term ($m^2.s^{-1}$). The right sides of both equations are similar, which confirms that the current equation is conservative in mass[43], supports the mass conservation property of the method already underlined by D'ortona[84] and Latva-Kokko[72]. In the density match case, ($\rho_1 = \rho_2$) the current equation Eq(65) becomes equivalent to the Allen-Cahn equation with the mobility given by:

$$M = \frac{p\Delta x}{2\rho c_s^2}. \tag{68}$$

Illustration

Let us now conduct a study in the density matched case to highlight the influence of the mobility parameter M, even if it cannot be defined in the general case. The influence of the mobility factor is investigated through the case of a flat interface. First of all, a convergence analysis is held to recover Eq. (65), and then the impact of the mobility on the dynamic of the interface is investigated.

The flat interface case is described as follow. The domain is a rectangular box with only few points ($Nx = 5$) in the short side, $Ny = \frac{L}{\Delta x}$ in the long side. The physical length

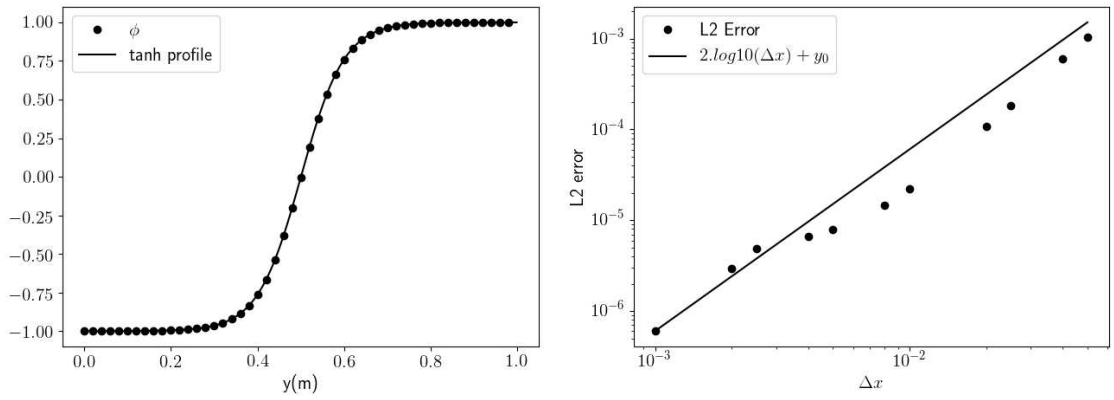

Figure 2: Visualization of a phase field profile after grid convergence (left). L2 error expressed as a function of the spatial step Δx compared with a straight line of slope=2 in a log-log scale.

of the domain is constant for all cases: $L = 1m$, and the space step Δx is used to set the mobility factor M though Eq. (68). The boundary conditions are set periodic for the long side (normal to the x direction) and to wall conditions for the short side (along the x direction). Two phases are initialized in two equal volume of space such as:

$$\begin{cases} \phi(y, t = 0) = -1 & 0 < y < \frac{L}{2} \\ \phi(y, t = 0) = 1 & \frac{L}{2} < y < L \end{cases} \tag{69}$$

Initially infinitely sharp. Due to the diffusive effect of the method, the interface widens under the effect of diffusion until it reaches its terminal thickness. First, the grid convergence is investigated. The characteristic length of the interface is set to $W = 0.1m$. As seen in Eq. (66), the solution at steady state should be a tangent hyperbolic profile. Then a $L2$ error can be defined as:

$$L2 = \frac{\sqrt{\sum_j^{Ny} (\phi(j) - \tanh \frac{j\Delta x - y_\epsilon}{W})^2}}{Ny} \tag{70}$$

It was stated in Eq. (65) that ϕ is solution of the Allen-Cahn equation with an error proportional to Δt^2 which is itself proportional to Δx^2. This can be verified by plotting the L2-error in a log-log diagram as in Fig. 2. The L2 error follows nicely the expected tendency, which supports the theoretical result of Eq. (65). To study the dynamics on the interface, the same set up is used chosing $W = 2.5\Delta x$. As previously, the case is performed for different values of Δx in order to compare the results with different values of the mobility factor M.

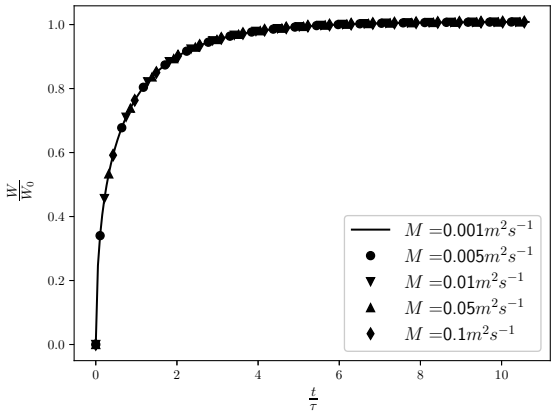

Figure 3: Time evolution of the non-dimensional interface thickness for different mobility factors M as a function of dimensionless time.

Assuming that the profile of the interface at any time corresponds to a tangent hyperbolic profile: $\phi(x,t) = tanh(\frac{x-x_\epsilon}{W(t)})$, the value of $W(t)$ can be determined at any time by proceeding through a least square algorithm. For clarity issues, W_0 now denotes the final value of the interface thickness. As the system only depends on W_0 and M, a non-dimensional time scale can be defined: $\tau_{int} = \frac{W_0^2}{2M}$. The evolution of the ratio W/W_0 is represented on Fig. (3) as a function of the dimensionless time: t/τ_{int}. It can be seen that the different profiles of interface thickening nicely superimpose on each other, evidencing that the evolution of the interface is driven by τ_{int} and W_0. Thanks to this analysis, it can be seen that the interface reaches 99% of its final thickness around $t = 5.6\tau_{int}$. It was pointed out earlier than the mobility factor (and consequently the characteristic time of interface thickening) is imposed by the numerical scheme, which could result in thickening of the interface slower than expected. To answer that issue, it is interesting to write τ_{int} as a function of the dimensionless interface final width $\tilde{W}_0$ defined as $\tilde{W}_0 = \frac{W_0}{\Delta x}$:

$$\tau_{int} = \frac{\tilde{W}_0 \rho c_s^2 \Delta t}{p} \tag{71}$$

In this equation it is straightforward that the characteristic time of thickening can be reduced by reducing the time step, i.e. by refining the mesh. It shows that the drawback that was highlighted earlier is actually not an issue for a fine enough mesh.

C. About the error term for a D2Q9 scheme

It has been known since the work of Holdych[91], that when the EOS of state is such as $p \neq \rho c_s^2$, an error appears in the stress tensor, leading to an equivalent momentum equation of the form (see derivation in Appendix C):

$$\partial_t \rho u_\alpha + \partial_\beta \left(\rho u_\alpha u_\beta + p\delta_{\alpha\beta} + p^\sigma_{\alpha\beta} - \mathcal{T}_{\alpha\beta} \right) = \Delta t \partial_\beta \left(Er_\alpha \delta_{\alpha\beta} \right) + O(\Delta t^2), \tag{72}$$

where the error term reads

$$Er_\alpha = \underbrace{-3(\tau_\nu - 1/2)\partial_\alpha \left((p - \rho c_s^2) u_\alpha \right) + \frac{3}{2} (\tau_\nu - \tau_b) \partial_\gamma \left((p - \rho c_s^2) u_\gamma \right)}_{\text{recursivity}} + \underbrace{(\tau_b - 1/2) \left(\partial_t (p - \rho c_s^2) + \partial_\gamma \left((p - \rho c_s^2) u_\gamma \right) \right)}_{\text{conservativity}}, \tag{73}$$

The error Er_α (C13) stems from two contributions:

- a lack of recursivity, pointed out by Malaspinas et al.[82],
- and the fact that p is not a conservative variable (e.g. $\partial_t p + \partial_\alpha p u_\alpha \neq 0$)

For implementation purposes, it is convenient to rewrite (C13) separating spatial and temporal derivatives as:

$$Er_\alpha = Er_t + Er_{Sp} \tag{74}$$

with

$$Er_{Sp} - 3(\tau_\nu - 1/2)\partial_\alpha \left((p - \rho c_s^2) u_\alpha \right) + \frac{3}{2} (\tau_\nu - \tau_b) \partial_\gamma \left((p - \rho c_s^2) u_\gamma \right) + (\tau_b - 1/2) \frac{\partial_\gamma (p - \rho c_s^2) u_\gamma}{2} \tag{75}$$

Two possible cures to the spatial error Er_{Sp} are proposed in the literature. Leclaire et al.[73] following the work of Che Sidick[92] proposed a modification of the equilibrium function that aims to correct the error term Er_{Sp} in the form of a forcing term. The second solution is to heal the recursivity of the scheme as proposed in the work of Li et al[79].

The first solution reportedly leads to discontinuity problems across sheared interfaces[78], as will be shown in the illustration hereafter. For this reason, the strategy by Li et al.[79] is

prefered, and S_{Sp} given in Eq. (53) can be recovered from:

$$\sum_i H_{\nu,i} S_{Sp,i} = 3\frac{\partial_y(p-\rho c_s^2)u_y - \partial_x(p-\rho c_s^2)u_x}{2} \tag{76}$$

$$\sum_i H_{b,i} S_{Sp,i} = \frac{\partial_\gamma(p-\rho c_s^2)u_\gamma}{2}. \tag{77}$$

To the authors' knowledge, the second error term Er_t has remained uncorrected up to date. This term has nonetheless a strong effect on the method stability, and can be recovered by enforcing:

$$\sum_i H_{b,i} S_{t,i} = \partial_t(p-\rho c_s^2), \tag{78}$$

or, equivalently, $\sum_i S_{t,i} H_{\alpha\beta,i} = \partial_t(p-\rho c_s^2)\delta_{\alpha\beta}$. Since Δt multiplies the error in Eq. (72), a first order approximation for the spatial derivative

$$\sum_i H_{b,i} S_{t,i}(x,t) = p(x,t+\Delta t) - p(x,t) - c_s^2\left(\rho(x,t+\Delta t) - \rho(x,t)\right) \tag{79}$$

is enough to recover a second-order accuracy in time, leading to the expression for S_t provided in Eq. (54).

Illustration

The test case is as follows: in a rectangular 2D box $Nx = 5$ and $Ny = 200$, two fluids coexist. The denser fluid 1 is located in a band of width $2a$ surrounded by two bands of width $b-a$ of the fluid 2, a and b being geometrical values given by $a = \frac{\Delta x Ny}{2}$ and $b = \frac{\Delta x Ny}{4}$. The system is invariant along the x-axis. Placing that the origin of the y-axis in the middle of the box, the initial phase field profile is given by $|y| < a$: $\phi = 1$ and when $a < |y| < b$: $\phi = -1$. The boundaries normal to the x-axis are set as walls, and the boundaries normal to the y-axis are periodic. Finally, a constant volumic force, which simulates a constant pressure gradient G, is applied. The expression of the force is given by $\vec{F} = G\vec{e_x}$. The norm of this force is given by $G = 9.81 kg.m^{-1}.s^{-2}$ An illustration is proposed in Fig. 4. Other usefull parameters that were used for the testcase are given afterward. The spatial step is set to $\Delta x = 0.001m$. The density ratio is set to 100, with densities of $\rho_{1,0} = 1 kg.m^{-3}$ and $\rho_{2,O} = 0.01 kg.m^{-3}$, the kinematic viscosity of the fluids are identical: $\nu_1 = \nu_2 = 1.666667 m^2.s^{-1}$, and the second viscosity is set equal to the shear viscosity: $\nu_{b,1} = \nu_{b,2} = \nu_1$. The speed of sound in both fluids is identical and equal to the speed of sound in air at ambient temperature, moreover

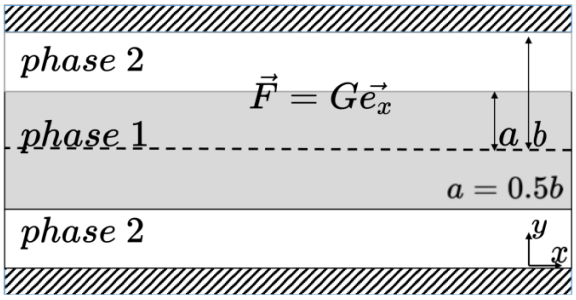

Figure 4: Two-phase Poiseuille flow case

the characteristic velocity c_s is set equal to the speeds of sound: $c_1 = c_2 = c_s = 347m.s^{-1}$. The lighter fluid is supposed to have no coherent forces, then $p_{\infty,2} = 0$, and $p_{\infty,1}$ is chosen to guarantee mechanical equilibrium between the phases, i.e., $p_{\infty,1} = (\rho_{1,0} - \rho_{2,0})c_s^2$. The surface tension is neglected $\sigma = 0$ which has no impact here, since the interfaces are planar in this Poiseuille flow. The interface thickness is set to $W = 1.6\Delta x$. The initial solution is implemented with a thick interface, i.e.:

$$\phi(x, y, 0) = \tanh\left(-\frac{|y| - a}{W}\right), \tag{80}$$

with W the interface thickness.

The analytical solution is known, a development is proposed by Huang and Lu[93]. Then the simulated field obtained can be compared to the analytical solution. Results are proposed in Fig. 5 where the analytical solution is also reported. *Two simulation are leaded. In the first one, referred as "model 1", Leclaire's scheme is implemented, i.e.* $S_{Sp} = 0$, $S_t = 0$ *and a correction term is added to the equilibrium function given in Eq.* (31) $f_i^{eq,(Leclaire)} = f_i^{eq} + \Phi_i$ *with the expression of* Φ *given in Leclaire et al.*[73]*. In the second one, referred as "model 2", the present scheme is used.* It is clearly visible that a non-physical velocity jump appears at the interface for the Leclaire's scheme, while the flow stays continuous across the interface with the proposed scheme.

V. VALIDATION AND RESULTS

A. Laplace test

One of the fundamental capability intended from a multiphase solver is the ability to accurately simulate surface tension. This behavior can be evaluated through the Laplace

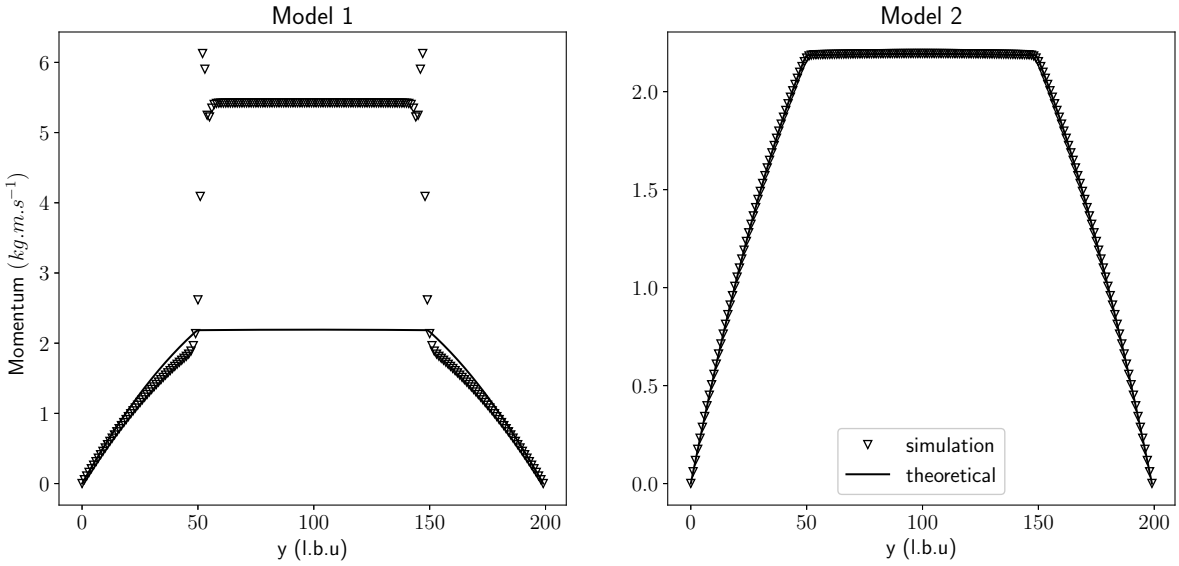

Figure 5: *Comparison between "model 1" inspired fom the scheme in Leclaire*[73] *(left), and "model 2" the present scheme inspired from Li*[79] *(right), for a two-phase Poiseuille flow at high density ratio case* (100)*. Both are compared with the theoretical solution (solid line)*

test. It consists in simulating a bubble or a droplet of a phase 1 in a quiescent atmosphere composed of phase 2. Due to surface tension, a pressure jump appears across the interface. In a 2D framework (which comes to simulate an infinite cylinder), the pressure jump is given by the following form of the Laplace law

$$p_1 - p_2 = \frac{\Gamma}{r} \tag{81}$$

r being the cylinder radius, p_1 the pressure outside the droplet/bubble, p_2 the pressure inside the droplet/bubble, Γ being the surface tension and r the radius of the cylinder. The test consists in comparing the value of given surface tension (in this case, the term σ in Eq. (45)), and the resulted pressure jump across the interface. This test was performed in a squared grid of size $Nx = 128$, $Ny = 128$, for a space step of $\Delta x = 0.0001m$. In this box, a bubble of radius r taking one value in the range of $(10, 15, 20, 25)\Delta x$, and with σ taking one value in $(1, 3, 5, 8)10^{-2}kg.s^{-2}$ (this relative narrow range of surface tension coefficient is motivated by the fact that the vast majority of practical cases falls into this interval, which excludes only extreme cases like the one implying mercury for instance). The density of the outside phase is the lowest and set to $\rho_2 = 1kg.m^{-3}$, while the other phase's density ρ_1 falls into the range: $(4, 10, 100, 1000)kg.m^{-3}$

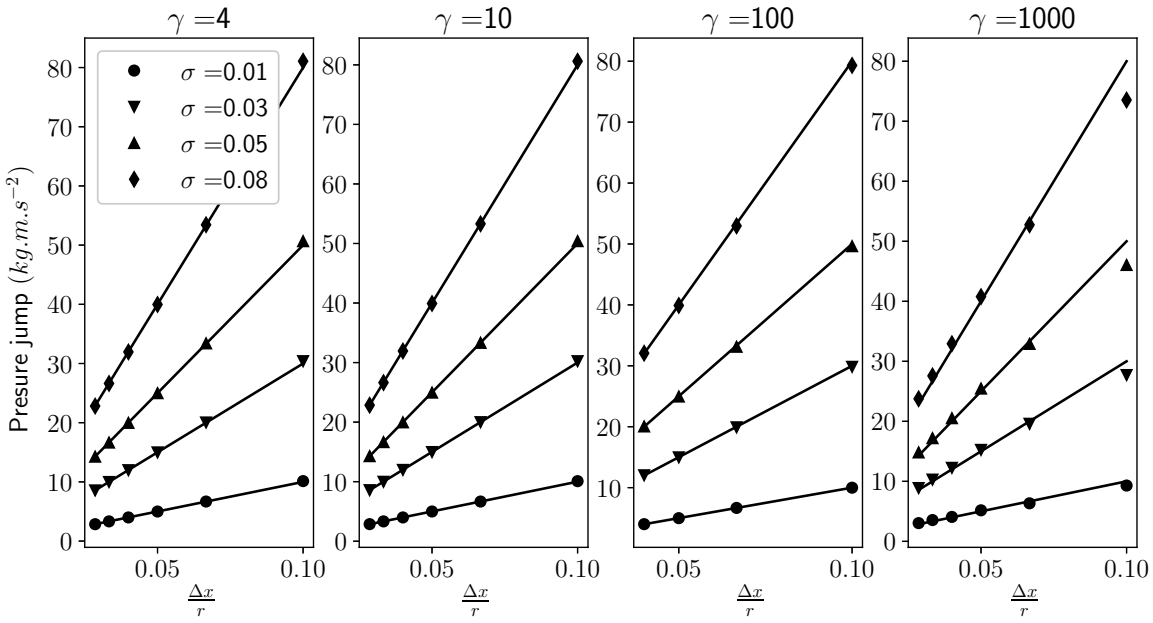

Figure 6: Laplace test for a range of surface tension σ, and radius r for different density ratios γ. The value of the pressure jump $p_1 - p_2$ (dots) can be compared with $\frac{\sigma}{r}$ (plain curve)

The test is initialized by setting:

$$\phi(x, y, 0) = -\tanh\left(\frac{\sqrt{(x - x_0)^2 + (y - y_0)^2)} - r}{W_0}\right) \tag{82}$$

$W_0 = 1.3\Delta x$ being the initial interface thickness and (x_0, y_0) the coordinates of the center of the box. The other parameters of the simulation are: $c_1 = c_2 = c_s = 347m.s^{-1}$, $W = 1.6\Delta x$, $\nu_1 = \nu_2 = \nu_{b,1} = \nu_{b,2} = 0.001m^2.s^{-1}$. The results of these multiple tests are proposed in Fig. 6. It can be seen that the relationship of proportionality between the pressure jump and $\Delta x/r$ is nicely recovered for a large range of density ratio, even as high as 1000. The accuracy of the pressure jump prediction is satisfying in most cases. Defining the relative error by:

$$E = 100\frac{|\sigma_{exp} - \sigma|}{\sigma} \quad \sigma_{exp} = (p_1 - p_2)r \tag{83}$$

E is found systematically under 2% and can be as low as 0.007% for density ratio of 4, 10 and 100. For a density ratio of 1000 the error increases between 7% and 8% for the case where the radius is $r = 10\Delta x$, and higher for surface tension, and remain reasonable for the other cases. The values for the relative error are given in Table I.

		Droplet radius (l.b.u.)			
γ	σ	10	15	20	25
4	0.01	1.36	0.207	0.0644	0.144
	0.03	1.34	0.201	0.0695	0.147
	0.05	1.34	0.201	0.0694	0.146
	0.08	1.34	0.202	0.0683	0.146
10	0.01	0.874	0.0195	0.168	0.164
	0.03	0.801	0.0502	0.177	0.167
	0.05	0.778	0.0578	0.180	0.169
	0.08	0.763	0.0617	0.181	0.170
100	0.01	0.101	0.148	0.0869	0.147
	0.03	0.550	0.490	0.140	0.244
	0.05	0.730	0.609	0.186	0.239
	0.08	0.861	0.683	0.223	0.221
1000	0.01	7.03	4.97	3.31	1.66
	0.03	7.62	2.02	1.59	2.07
	0.05	7.89	1.31	1.80	2.58
	0.08	8.09	1.12	1.95	2.91

Table I: Relative error E calculated with Eq(83) for different density ratios (γ), surface tension (σ in $kg.s^{-2}$) and for different droplet radii (expressed in l.b.u., i.e., as multiples of Δx)

B. Oscillating droplet

If the previous test case allowed to evaluate the capability of the model to simulate surface tension in a static case, a dynamic case is now evaluated. The case of an ellipsoidal oscillating bubble is chosen. As in the previous case a denser phase 1 is put into a quiescent atmosphere composed of phase 2. The final shape of this droplet must be spherical. As the droplet is not initially in its equilibrium shape, surface tension initiates the contraction of the bubble to its final shape, but due to its own inertia, the bubble tends to oscillate around the spherical shape until viscous effects degrade the interface motion. The oscillation of a

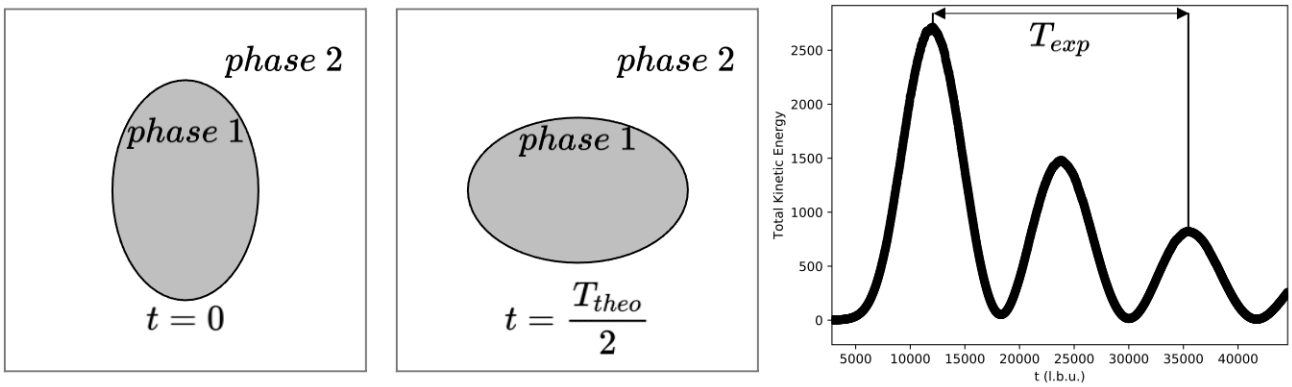

Figure 7: Illustration of an oscillating ellipsoidal droplet between initial state (left) and half period state (centre). Time evolution of kinetic energy curve (right)

droplet has been studied by Lord Rayleigh[94], who proposed a theoretical value for a cylinder oscillation period when excited through different modes. When adapted to a 2D circle, this period is:

$$T_{theo} = 2\pi\sqrt{\frac{(\rho_1 + \rho_2)r^3}{6\Gamma}} \tag{84}$$

The case is described as follows: in a squared box ($Nx = Ny = 128$), an ellipsoidal droplet is initialized in a quiescent atmosphere. The initial profile is given by:

$$\phi(x, y, 0) = -\tanh\frac{\sqrt{\frac{(x-x_0)^2}{a^2} + \frac{(y-y_0)^2}{b^2}} - R}{W_0} \tag{85}$$

where a and b are the semi-axis length of the ellipsoid, given by $a = \sqrt{\frac{3}{2}}$, $b = 1/a$, $W_0 = 1.1\Delta x$ is the initial interface width. R is the radius of the disc with the same area of the ellipse (i.e., the area of the ellipse is πR^2). The other parameters are: $\Delta x = 0.0001m$ $\nu_1 = \nu_2 = \nu_{b,1} = \nu_{b,2} = 0.0002m^2s^{-1}$, $W = 1.6\Delta x$, $\rho_2 = 1kg.m^{-3}$, $c_1 = c_2 = 347m.s^{-1}$. All boundaries are periodic. An illustration of the setup is proposed Fig. 7.

As explained by Rayleigh[94], the phenomenon of the oscillating droplet consists in a periodic transfer of energy between the kinetic energy and the surface tension energy. When the droplet is totally deformed, the kinetic energy is minimum and the surface tension energy is minimum when the sphere is into a spherical shape. As a consequence, the period of the phenomenon can easily be measured by plotting the kinetic energy of the system. The total

kinetic energy (K_E) of the droplet is calculated through:

$$K_E = \sum_{i,j}^{N_x,N_y} \rho \frac{1+\phi}{2} \frac{u_x^2 + u_y^2}{2} \tag{86}$$

An example of this function of time is given in Fig. 7. The period can then be determined by measuring the time between the extrema of this curve. From this measured period (noted T_{exp}), an experimental surface tension can be defined by inverting Eq(84):

$$\sigma_{exp} = \left(\frac{2\pi}{T_{exp}}\right)^2 \frac{(\rho_1 + \rho_2) r^3}{6} \tag{87}$$

Then a relative error can be defined:

$$Er = 100 \frac{|\sigma_{exp} - \sigma|}{\sigma} \tag{88}$$

This analysis has been performed for different values of radii ($r = (15, 20, 25)\Delta x$), density ratio ($\gamma = (4, 10, 100)$ giving $\rho_2 = 1 kg.m^{-3}$) and surface tension ($\sigma = (0.05, 0.07, 0.08)$). More over, this test case is also the opportunity to appreciate the gain in terms of numerical stability coming from the temporal correction (the counterpart of the source term given in Eq. (54)). Then the simulation will be performed twice, one with $S_t = 0$ (no correction) and one with S_t defined as in Eq. (54). The results are compiled in Table II. It should be noted that the range of radii and surface tension is smaller than for the Laplace test. This is due to the fact that all ellipsoidal droplets do not oscillate. In Fig. 7, it can be seen that the envelope of the kinetic energy oscillations decreases with time due to viscous dissipation. When this decrease is too sharp (i.e., when the characteristic time of the dissipation is shorter than the period of oscillation), the droplet does not oscillate. For this reason, systems with surface tension lower than $0.05 kg.s^{-2}$, radii lower than $15\Delta x$, or density ratio of 1000 are not presented in this study. A possibility to simulate the oscillation of the cases would be to reduce the viscosity. In this study, it was set to $\nu = 2.10^{-4} m.s^{-2}$, but a lower value would lead to unstable behaviors.

First of all, it can be seen that the temporal correction allows a better robustness of the method at high density ratio. For a density ratio of 100, the absence of temporal correction implies the non-stability of the method. It should also be noted that, despite the absence of cases at a ratio density of 1000, they were simulated and found numerically unstable without the temporal correction. Otherwise, it can be seen that when the method is stable enough,

		$\gamma = 4$				$\gamma = 10$				$\gamma = 100$			
		Correction		No correction		Correction		No correction		Correction		No correction	
radius	σ	σ_{exp}	Er	σ_{exp}	Er	σ_{exp}	Er	σ_{exp}	Er	σ_{exp}	Er	σ_{exp}	Er
	0.05	0.042	9.2	0.042	9.2	0.046	4.79	0.046	4.38	-	-	crash	
15	0.07	0.059	8.56	0.059	8.98	0.065	3.57	0.036	40.0	-	-	crash	
	0.08	0.068	8.38	0.068	8.80	0.075	4.79	0.040	42.3	-	-	crash	
	0.05	0.043	7.94	0.043	8.35	0.046	4.16	0.046	4.16	0.035	19.9	crash	
20	0.07	0.061	7.41	0.061	7.41	0.065	3.59	0.065	3.59	0.054	14.0	crash	
	0.08	0.070	7.28	0.070	7.28	0.075	3.42	0.075	3.22	0.065	10.8	crash	
	0.05	0.043	7.58	0.043	7.78	0.046	4.41	0.046	4.21	0.16	43.4	crash	
25	0.07	0.061	6.89	0.061	7.09	0.065	3.83	0.065	3.66	0.065	3.73	crash	
	0.08	0.070	6.74	0.070	6.74	0.074	3.67	0.075	3.47	0.073	4.72	crash	

Table II: Oscillation of an ellipsoidal droplet: comparison between expected surface tension σ and experimental value σ_{exp} The symbol "$-$" underlines a lack of oscillation and "$crash$" a lack of numerical stability

the performances in terms of prediction are pretty similar in most cases. The trend seems to be that the higher surface tension is, the more precise the method is and the larger the radius of the droplet is, the more precise the method is. These two values are directly linked to the amplitude of the oscillation: high oscillations lead to better precision. This explains the poor capability of prediction in the case $\gamma = 100$ for $r = 20$ and $r = 25$ for $\sigma = 0.05$: in all these cases, the oscillation is particularly weak, and the droplet is nearly not oscillating. In favorable cases, the performances of the method are very good since it can go as low as a 3.47% error. Giving the fact that Eq. (84) was obtained by assuming an inviscid system, it is reasonable to think that this performances could be enhanced in a less viscous simulation.

C. Rayleigh-Taylor instability

Previous cases showed that the method could actually predict accurately the behavior of an interface. Then the numerical robustness of the method can be interrogated. The Rayleigh Taylor instability is a good case to investigate it. This instability appears when

a heavier fluid is put over a lighter fluid and when both of them are under the influence of a gravitational field. Under certain condition, the interface is unstable which turns a small disturbance into non-linear behaviors and can lead to break-up for high Reynolds Number (Re) cases. In order to compare with the literature, the setup of He et al[95] is reproduced. In a rectangular box (Nx=256, Ny=1024) the, a fluid of density $\rho_1 = 3kg.m^{-3}$ is put up on a lighter fluid $\rho_2 = 1kg.m^{-3}$. The box width is $L = \Delta x Nx$. Defining the Atwood number (At) by:

$$\frac{\rho_1 - \rho_2}{\rho_1 + \rho_2} \tag{89}$$

this choice of density leads to $At = 0.5$. The phase field is initiated as:

$$\phi(x, y, 0) = \tanh \frac{y - y_0 - 0.2L \cos\left(\frac{-2\pi x}{L}\right)}{W_0} \tag{90}$$

y_0 being the vertical coordinate of the center of the box. As it can be seen, a single-mode initial perturbation is imposed. Moreover, a volume force us applied, taking the form:

$$\vec{F} = -\rho g \vec{e_y} \tag{91}$$

$\vec{e_y}$ being the vertical direction. In this case, no surface tension is included, then $\sigma = 0$. A characteristic velocity is given by $U_0 = \sqrt{Lg}$. In He et al.[95], the characteristic non-dimensional velocity is set to the value of 0.04 which gives $U_0 = 0.04\frac{\Delta x}{\Delta t}$ in the present study, as well as $L = 56.1m$. From this velocity, a Reynolds number can be determined:

$$Re = \frac{U_0 L}{\nu} = 2048 \tag{92}$$

Leading to the kinematic viscosity $\nu = 0.643m^2.s^{-1}$. Finally, a dimensionless time can be defined as:

$$t^* = t\sqrt{\frac{g}{L}} \tag{93}$$

The result of the simulation is illustrated in Fig. 8 The flow profiled obtained is similar to the one obtained through the HCZ method (He et al[95]). Compared to HCZ method, the present work tends to accentuate the atomisation process since more little structures appear. This results underline the capability of the method to handle high Reynold flows for a colour gradient method without the necessity to set a high bulk viscosity. More over, as expected from a diffuse interface method, the break up into small structures, even in structures as complex as in the present work, does not affect the numerical stability.

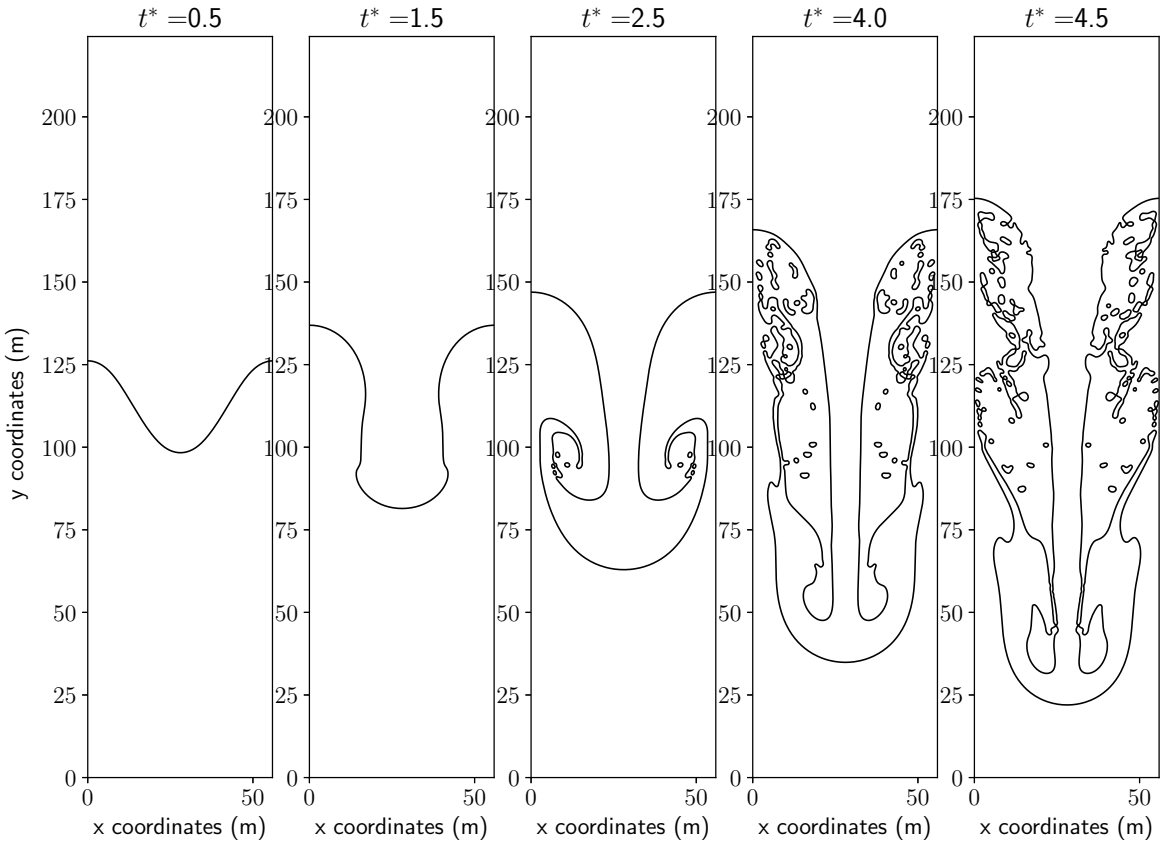

Figure 8: Rayleigh-Taylor instability at various characteristic times t^*, Reynolds number is $Re = 2048$

VI. CONCLUDING REMARKS

A new, improved formulation of the Color gradient method[67] has been proposed, presenting the following characteristics:

- The stream & collide algorithm structure[66] is fully preserved and only knowledge of first neighbors is required, allowing efficient and scalable implementation.
- The model is derived for an arbitrary equation of state, relieving the unphysical relation between density and sound speed ratios (10) present in the original formulation[67],
- A novel fourth order operator is used, allowing to limit spurious currents arising from isotropy defects;

- A novel temporal correction, required for use of arbitrary equation of states, is proposed.

The model was then validated based on static and oscillating droplets up to density ratios of 1000, on a two-phase Poiseuille flow and on a Rayleigh Taylor instability at Re=2048. In a future work, the present approach will be extended to non-isothermal flows.

ACKNOWLEDGEMENTS

The authors wish to acknowledge Gabriel Farag, Gauthier Wissocq, Florian Renard, Thomas Astoul, Minh NGuyen, Thomas Laroche and Thibault Gioud for fruitful discussions. This work has received financial support from Safran Tech. Léa Voivenel and Stefano Puggeli from Safran Tech are also acknowledged for project coordination. This project has received funding from the European Union's Horizon 2020 research and innovation programme under grant Agreement number 766264.

Appendix A: Hermite definitions

The Hermite polynomials are defined as:

$$H_{0,i} = 1 \tag{A1}$$

$$H_{\alpha,i} = \xi_{\alpha,i} \tag{A2}$$

$$H_{\alpha\beta,i} = \xi_{\alpha,i}\xi_{\beta,i} - c_s^2\delta_{\alpha\beta} \tag{A3}$$

$$H_{\alpha\beta\gamma,i} = \xi_{\alpha,i}\xi_{\beta,i}\xi_{\gamma,i} - c_s^2\left(\xi_\alpha\delta_{\beta\gamma} + \xi_\beta\delta_{\alpha\gamma} + \xi_\gamma\delta_{\alpha\beta}\right) \tag{A4}$$

$$H_{\alpha\beta\gamma\mu,i} = \xi_{\alpha,i}\xi_{\beta,i}\xi_{\gamma,i}\xi_{\mu,i} \tag{A5}$$

$$-c_s^2(\xi_{\alpha,i}\xi_{\beta,i}\delta_{\gamma\mu} + \xi_{\alpha,i}\xi_{\gamma,i}\delta_{\beta\mu} + \xi_{\alpha,i}\xi_{\mu,i}\delta_{\beta\gamma} \tag{A6}$$

$$+\xi_{\beta,i}\xi_{\gamma,i}\delta_{\alpha\mu} + \xi_{\beta,i}\xi_{\mu,i}\delta_{\alpha\gamma} + \xi_{\gamma,i}\xi_{\mu,i}\delta_{\alpha\beta}) \tag{A7}$$

$$+c_s^4(\delta_{\alpha\beta}\delta_{\gamma\mu} + \delta_{\alpha\gamma}\delta_{\beta\mu} + \delta_{\alpha\mu}\delta_{\beta\gamma}) \tag{A8}$$

Two additional polynomials are used and are compositions of Hermite's polynomial:

$$H_{\nu,i} = \frac{H_{xx,i} - H_{yy,i}}{2} \tag{A9}$$

$$H_{b,i} = \frac{H_{xx,i} + H_{yy,i}}{2} \tag{A10}$$

H_ν is linked to shear stress and H_b is linked to bulk viscosity.

Appendix B: Taylor Expansion

In this appendix, the equivalent equation of the Lattice Boltzmann algorithm are derived up to the order 3 following the method presented in the work of Dubois[87]. It shows the equation that is solved by the moments of the main density population f_i. As Dubois's development takes place in a Multiple Relaxation Time (MRT) framework, the moments m_j of the distribution function f_i are defined as

$$\sum_i M_{ji} f_i = m_j \tag{B1}$$

with M the transformation matrix from the population function basis to the moments function basis. To fit the MRT formalism, a specific relaxation time must also be attributed to each moment. In the method presented in the main text, a regularized collision model is used which can be translated in a MRT framework. the M matrix the Hermite polynomial basis and is given by:

$$M_{\alpha,i} = H_{\alpha,i} \tag{B2}$$

$$M_{\alpha\beta,i} = H_{\alpha\beta,i} \tag{B3}$$

$$M_{b,i} = \frac{H_{xx,i} + H_{yy,i}}{2} \tag{B4}$$

$$M_{\nu,i} = \frac{H_{xx,i} - H_{yy,i}}{2} \tag{B5}$$

$$M_{\alpha\beta\gamma,i} = H_{\alpha\beta\gamma,i} \tag{B6}$$

$$M_{\alpha\beta\gamma\mu,i} = H_{\alpha\beta\gamma\mu,i} \tag{B7}$$

Relaxation times must be attributed to each moments, in the regularized framework, this comes as: $\tau_{xy} = \tau_\nu = \frac{\rho\nu}{p\Delta t} + \frac{1}{2}$, $\tau_b = \frac{\rho\nu_b}{p\Delta t} + \frac{1}{2}$ and other relaxation times are set to 1, i.e.: $\tau_0 = \tau_\alpha = \tau_{\alpha\beta\gamma} = \tau_{\alpha\beta\gamma\mu} = 1$. This formulation not being symmetrical between x and y coordinates can complicate the formulation. For this reason, in this development, the formulation will be given form $M_{4i} = H_{xx,i}$ and $M_{5i} = H_{yy,i}$, and then $\tau_{\alpha\beta} = \tau_\nu$. While the ideas of the calculation are conserved, the formulation is way simpler. For the critical phases, some results in the based used in the main text will be given so the interested reader can recover those results easily. The inverse-matrix of M is noted M^{-1} si that:

$$f_j = \sum_i M^{-1}_{ji} m_i \tag{B8}$$

In this framework, the formulation of the LBM algorithm has to be slightly modified:
Streaming step

$$f_i(x, t + \Delta t) = f_i^*(x - \xi_i \Delta t, t) \tag{B9}$$

Collision step:

$$m_j^* = m_j^{eq} + (1 - \frac{1}{\tau_j}) \left(m_j - m_j^{eq} + \frac{1}{2} S_j \right) + \frac{1}{2} S_j \tag{B10}$$

As can be seen, a source term is present in this collision step. Note that if this source term is aimed to introduce a volumic force, then the 1st moment of f_i (i.e., $m_\alpha = \sum_i \xi_{\alpha,i} f_i$) is no longer equal to the momentum, but is linked with the volumic force through $m_\alpha = m_\alpha^{eq} - \frac{\Delta t}{2} F_\alpha$. It is actually not necessary to give this relationship as a necessary condition to recover the desired macroscopic equations, this relationship actually comes naturally at the end of this development. To illustrate that, until the last steps of this development, the value of the 1^{st} moment of f_i will not be specified. In agreement with Dubois's[87], this notation is adopted: $\Lambda_{j,\alpha}^k = \sum_i M_{ji} \xi_{\alpha,i} M_{ik}^{-1}$ and similarly: $\Lambda_{j,\alpha\beta}^k = \sum_i M_{ji} \xi_{\alpha,i} \xi_{\beta,i} M_{ik}^{-1}$, and $\Lambda_{j,\alpha\beta\gamma}^k = \sum_i M_{ji} \xi_{\alpha,i} \xi_{\beta,i} \xi_{\gamma,i} M_{ik}^{-1}$. The following relationship will be used:

$$\Lambda_{j,\alpha\beta}^l = \sum_k (\Lambda_{j\alpha}^k \Lambda_{kl}^\beta) \tag{B11}$$

Eq .(B10) can be manipulated to obtain

$$m_j - m_j^* = \frac{1}{\tau_j} \left(m_j - m_j^{eq} \right) - \left(1 - \frac{1}{2\tau_j} \right) S_j \tag{B12}$$

Using Taylor expansion, Eq. (B9) can be extended to:

$$\begin{aligned} & f_i(x,t) + \Delta t \partial_t f_i(x,t) + \tfrac{\Delta t^2}{2} \partial_t^2 f_i(x,t) \\ = & f_i^*(x,t) - \Delta t \xi_{\alpha,i} \partial_\alpha f_i^*(x,t) + \tfrac{\Delta t^2}{2} \xi_{\alpha,i} \xi_{\beta,i} \partial_{\alpha\beta} f_i^*(x,t) + O(\Delta t^3) \end{aligned} \tag{B13}$$

At the first order in Δt the last equation becomes $f_i = f_i^* + O(\Delta t)$. This equation is true for all the microscopic velocities i, then by using equation Eq. (B1):

$$m_j = m_j^* + O(\Delta t) \tag{B14}$$

By injecting this relationship in Eq. (B12) and after small manipulations, it comes:

$$m_j = m_j^{eq} + \left(\tau_j - \frac{1}{2} \right) S_j + O(\Delta t) \tag{B15}$$

1. 1^{st} Order

Developed at the order $O(\Delta t^2)$, and integrated in the moment space, Eq. (B13) becomes:

$$(m_j - m_j^*) = -\Delta t \left(\partial_t m_j + \partial_\alpha \left(\sum_k \Lambda_{j,\alpha}^k m_k^* \right) \right) + O(\Delta t^2) \tag{B16}$$

Using the collision relationship, Eq. (B12), it comes:

$$\partial_t m_j + \partial_\alpha \left(\sum_k \Lambda_{j,\alpha}^k m_k^* \right) = \frac{1}{\Delta t} \left(\left(1 - \frac{1}{2\tau_j} \right) S_j - \frac{m_j - m_j^{eq}}{\tau_j} \right) \tag{B17}$$

For $j = 0$, the previous equation can be simplified (giving $m_0 = \rho$, $m_0^{eq} = \rho$ and $S_0 = 0$). Moreover, the term $\Lambda_{j,\alpha}^k$ can be determined. Given $M_{0,i} = 1$ then $M_{ji}\xi_{\alpha,i} = M_{\alpha,i}$. Then:

$$\begin{aligned} \sum_k \Lambda_{j,\alpha}^k m_k^* = \sum_{ik} M_{ji}\xi_{\alpha,i} M_{ki}^{-1} m_k^* = \sum_k \left(\sum_i M_{\alpha,i} M_{ik}^{-1} \right) m_k^* \\ = \sum_k \delta_{\alpha k} m_k^* = m_\alpha^* \end{aligned} \tag{B18}$$

By expressing m_j^* in term of m_j^{eq} and S_j through Eq. (B14) and Eq. (B15) it comes:

$$\partial_t m_0 + \partial_\alpha \left(m_\alpha^{eq} + \left(\tau_\alpha - \frac{1}{2} \right) S_\alpha \right) = O(\Delta t) \tag{B19}$$

For $j = \alpha$, the sum term can also be simplified. M_{ji} becomes $M_{\alpha i}$. Then $M_{\alpha i}\xi_{\beta i} = \xi_\alpha \xi_\beta$. Then the product $\xi_\alpha \xi_\beta$ must be expressed in terms of vectors of the matrix M:

$$\xi_\alpha \xi_\beta = M_{\alpha\beta,i} + c_s^2 H_{0,i} \delta_{\alpha\beta} \tag{B20}$$

In the case of the polynomial basis used in the main text, this expression is slightly more complicated and must be detailed for the different values of α and β:

$$\xi_x \xi_y = M_{xy,i} \tag{B21}$$

$$\xi_x^2 = M_{b,i} + M_{\nu,i} + M_{0,i} c_s^2 \tag{B22}$$

$$\xi_y^2 = M_{b,i} - M_{\nu,i} + M_{0,i} c_s^2 \tag{B23}$$

As a consequence, $\Lambda_{j,\alpha}^k$ can be detailed:

$$\begin{aligned} \sum_k \Lambda_{j,\alpha}^k m_k^* = \sum_{ik} M_{ji}\xi_{\beta,i} M_{ki}^{-1} m_k^* = \sum_k \left(\sum_i M_{\alpha\beta,i} + c_s^2 M_{0i}\delta_{\alpha\beta} \right) m_k^* \\ = m_{\alpha\beta}^* + m_0^* c_s^2 \delta_{\alpha\beta} \end{aligned} \tag{B24}$$

Then using previous relationships Eqs. (B14)(B15), the Eq. (B17) can be expressed for $j = \alpha$:

$$\partial_t m_\alpha + \partial_\beta \left(m^{eq}_{\alpha\beta} + c_s^2 m_0^{eq} \delta_{\alpha\beta} + \left(\tau_{\alpha\beta} - \frac{1}{2} \right) S_{\alpha\beta} \right) = \frac{1}{\Delta t} \left(\left(1 - \frac{1}{2\tau_\alpha} \right) S_\alpha - \frac{m_\alpha - m^{eq}_\alpha}{\tau_\alpha} \right) + O(\Delta t) \quad \text{(B25)}$$

From the previous equation, a condition between the first moments m^{eq}_α, m_α and S_α stands out:

$$F_\alpha = \frac{1}{\Delta t} \left(\left(1 - \frac{1}{2\tau_\alpha} \right) S_\alpha - \frac{m_\alpha - m^{eq}_\alpha}{\tau_\alpha} \right) \quad \text{(B26)}$$

To conclude with the first order, the following relationships can be obtained by manipulating both Eqs. (B15)(B10):

$$m^*_j = m^{eq}_j + (\tau_j - 1/2)\, S_j - \Delta t(\tau_j - 1) \left(\partial_t m_j + \partial_\alpha \left(\sum_k \Lambda^k_{j,\alpha} m^*_k \right) \right) + O(\Delta t^2) \quad \text{(B27)}$$

$$m_j = m^{eq}_j + (\tau_j - 1/2)\, S_j - \Delta t \tau_j \left(\partial_t m_j + \partial_\alpha \left(\sum_k \Lambda^k_{j,\alpha} m^*_k \right) \right) + O(\Delta t^2) \quad \text{(B28)}$$

2. 2^{nd} order

Eq. (B13) when fully integrated into the moments space is given by:

$$\frac{1}{\tau_j}(m_j - m^{eq}_j) - \left(1 - \frac{1}{2\tau_j} \right) S_j = -\Delta t \left(\partial_t m_j + \partial_\alpha \left(\sum_k \Lambda^k_{j,\alpha} m^*_k \right) \right) - \frac{\Delta t^2}{2} \left(\partial_t^2 m_j - \partial_{\alpha\beta} \left(\sum_k \Lambda^k_{j,\alpha\beta} m^*_k \right) \right) + O(\Delta t^3) \quad \text{(B29)}$$

Then this equation must be reduced for the two moments of interest: $j = 0$ and $j = \alpha$. First of all $\Lambda^k_{j,\alpha\beta}$ must be determined for $j = 0$. Giving $M_{ji} = 1$, it reduces to: $\Lambda^k_{0,\alpha\beta} = \sum_{ik} \xi_{\alpha,i} \xi_{\beta,i} M^{-1}_{ik}$ which has already been calculated (Eq(B20))

$$\Delta t \left(\partial_t m_0 + \partial_\alpha m^*_\alpha \right) + \frac{\Delta t^2}{2} \left(\partial_t^2 m_0 - \partial_{\alpha\beta} \left(m^*_{\alpha\beta} + c_s^2 m^*_0 \delta_{\alpha\beta} \right) \right) = O(\Delta t^2) \quad \text{(B30)}$$

By expanding $\partial_t^2 m_0$ using Eq(B19), and by expanding m^*_α, the previous equation becomes:

$$\partial_t m_0 + \partial_\alpha \left(m^{eq}_\alpha + (\tau_\alpha - 1/2)\, S_\alpha \right) - \Delta t \left(\tau_\alpha - 1/2 \right) \left(\partial_t m_\alpha + \partial_\beta \left(m^*_{\alpha\beta} + c_s^2 m^*_0 \delta_{\alpha\beta} \right) \right) = O(\Delta t^2) \quad \text{(B31)}$$

After few manipulations implying Eq. (B25), and by integrating the relationship between the volumic force and the 1^{st} moments Eq(B26):

$$\partial_t m_0 + \partial_\alpha \left(m_\alpha + \frac{\Delta t}{2} F_\alpha \right) = O(\Delta t^2) \tag{B32}$$

From the previous equation, it comes in a straightforward way that to ensure the mass conservation principle, the first moments of the density population must respect:

$$m_\alpha + \frac{\Delta t}{2} F_\alpha = \rho u_\alpha \tag{B33}$$

which is the condition often found in the literature[96].

The same work should now be done for $j = \alpha$. Eq(B29) becomes

$$\partial_t m_\alpha + \partial_\beta \left(m^*_{\alpha\beta} + c_s^2 m_0^* c_s^2 \delta_{\alpha\beta} \right) + \Delta t \left(\partial_t^2 m_\alpha - \partial_{\alpha\beta} \left(\sum_k \Lambda^k_{\alpha,\beta\gamma} m_k^* \right) \right) = F_\alpha + O(\Delta t^2) \tag{B34}$$

Giving that $M_{\alpha,i} = \xi_{\alpha,i}$ and that:

$$\xi_\alpha \xi_\beta \xi_\gamma = M_{\alpha\beta\gamma} + c_s^2 (M_\alpha \delta_{\beta\gamma} + M_\beta \delta_{\alpha\gamma} + M_\gamma \delta_{\alpha\beta}) \tag{B35}$$

It comes: $\sum_k \Lambda^k_{\alpha,\beta\gamma} m_k^* = m^*_{\alpha\beta\gamma} + c_s^2 (m^*_\alpha \delta_{\beta\gamma} + m^*_\beta \delta_{\alpha\gamma} + m^*_\gamma \delta_{\alpha\beta})$ Using Eq(B27) to expand $m^*_{\alpha\beta}$ and Eq(B25) to expand $\partial_t^2 m_\alpha$, the following equation comes:

$$\begin{aligned} \partial_t \left(m_\alpha + \frac{\Delta t}{2} f_\alpha \right) + \partial_\beta \left(m^{eq}_{\alpha\beta} + m_0^{eq} c_s^2 \delta_{\alpha\beta} + ((\tau_{\alpha\beta} - 1/2) S_{\alpha\beta}) \right) - \\ \Delta t \left(\tau_{\alpha\beta} - 1 \right) \partial_\beta \left(\partial_t m_{\alpha\beta} + \partial_\gamma \sum_k \Lambda^k_{\alpha\beta,\gamma} m_k^* \right) \\ - \frac{\Delta t}{2} \left(\partial_t \left(m^*_{\alpha\beta} + m_0^* c_s^2 \delta_{\alpha\beta} \right) + \partial_\gamma \left(m^*_{\alpha\beta\gamma} + c_s^2 (m^*_\alpha \delta_{\beta\gamma} + m^*_\beta \delta_{\alpha\gamma} + m^*_\gamma \delta_{\alpha\beta}) \right) \right) \\ = F_\alpha + O(\Delta t^2) \end{aligned} \tag{B36}$$

Giving $M_{\alpha\beta,i} \xi_{\gamma,i} = M_{\alpha\beta\gamma,i} + c_s^2 \left(M_{\alpha,i} \delta_{\beta\gamma} + M_{\beta,i} \delta_{\alpha\gamma} \right)$ and by including Eq(B19), it comes:

$$\begin{aligned} \partial_t \left(m_\alpha + \frac{\Delta t}{2} F_\alpha \right) + \partial_\beta \left(m_{\alpha\beta} + m_0^{eq} c_s^2 \delta_{\alpha\beta} + (\tau_{\alpha\beta} - 1/2) S_{\alpha\beta} \right) \\ = \Delta t (\tau_{\alpha\beta} - 1/2) \Pi_{\alpha\beta} + f_\alpha + O(\Delta t^2) \end{aligned} \tag{B37}$$

with $\Pi_j = \partial_t m_j + \partial_\alpha \sum_k (\Lambda^k_{j,\alpha} m_k^*)$. It is also useful to define:

$$\Pi_j^{eq} = \partial_t \left(m_j^{eq} + (\tau_j - 1/2) S_j \right) + \partial_\alpha \sum_k \left(\Lambda^k_{j,\alpha} \left(m_k^{eq} + (\tau_k - 1/2) S_k \right) \right) \tag{B38}$$

Noting that: $\Pi_{\alpha\beta} = \Pi^{eq}_{\alpha\beta} + O(\Delta t)$, the equation of conservation of momentum can be written as:

$$\partial_t \left(m_\alpha + \frac{\Delta t}{2} F_\alpha \right) + \partial_\beta \left(m_{\alpha\beta} + m_0^{eq} c_s^2 \delta_{\alpha\beta} + (\tau_{\alpha\beta} - 1/2)\, S_{\alpha\beta} \right) = \Delta t(\tau_{\alpha\beta} - 1/2)\Pi^{eq}_{\alpha\beta} + F_\alpha + O(\Delta t^2) \quad \text{(B39)}$$

To conclude with the 2^{nd} order, the following relationships can be obtained by manipulating Eqs. (B10, B29):

$$m_j^* = m_j^{eq} + (\tau_j - 1/2)\, S_j - \Delta t\, (\tau_j - 1) \left(\partial_t m_j + \partial_\alpha \left(\sum_k \Lambda^k_{j,\alpha} m_k^* \right) \right) - \frac{\Delta t^2}{2} \Delta t\, (\tau_j - 1) \left(\partial_t^2 m_j - \partial_{\alpha\beta} \left(\sum_k \Lambda^k_{j,\alpha\beta} m_k^* \right) \right) + O(\Delta t^3) \quad \text{(B40)}$$

Using Eq(B11), the last term can be manipulated:

$$\begin{aligned} &\partial_t^2 m_j - \partial_{\alpha\beta} \left(\sum_k \Lambda^k_{j,\alpha\beta} m_k^* \right) \\ &\quad = \partial_t^2 m_j + \underbrace{\partial_t \partial_\alpha \Lambda^l_{j,\alpha} m_l^* - \partial_t \partial_\alpha \Lambda^l_{j,\alpha} m_l}_{=O(\Delta t)} - \partial_{\alpha\beta} \sum_{kl} \Lambda^l_{j,\alpha} \Lambda^k_{j,\alpha\beta} m_k^* + O(\Delta t) \\ &\quad = \partial_t \Pi_j - \partial_\alpha \Lambda^l_{j,\alpha} \Pi_l + O(\Delta t) = \partial_t \Pi_j^{eq} - \partial_\alpha \Lambda^l_{j,\alpha} \Pi_l^{eq} + O(\Delta t) \end{aligned} \quad \text{(B41)}$$

By extending $\partial_t m_j$ and $\partial_\alpha \Lambda^k_{j,\alpha} m_k *$ using Eq. (B27) and Eq. (B28), Eq. (B40) reduces to:

$$m_j^* = m_j^{eq} + (\tau_j - 1/2) S_j - \Delta t\, (\tau_j - 1)\, \Pi_j^{eq} - \Delta t^2\, (\tau_j - 1) \left((\tau_j - 1/2) \partial_t \Pi_j^{eq} + \partial_\alpha \sum_k (\tau_k - 1/2) \Lambda^k_{j,\alpha} \Pi_k^{eq} \right) + O(\Delta t^3) \quad \text{(B42)}$$

3. 3^{rd} Order

Eq. (B13) can be extended to an additional order and then integrated to the moment space which gives:

$$\frac{1}{\tau_j}(m_j - m_j^{eq}) - \left(1 - \frac{1}{2\tau_j}\right) S_j = -\Delta t \left(\partial_t m_j + \partial_\alpha \left(\sum_k \Lambda_{j,\alpha}^k m_k^*\right)\right) - \frac{\Delta t^2}{2}\left(\partial_t^2 m_j - \partial_{\alpha\beta}\left(\sum_k \Lambda_{j,\alpha\beta}^k m_k^*\right)\right) - \frac{\Delta t^3}{6}\left(\partial_t^3 m_j + \partial_{\alpha\beta\gamma}\left(\sum_k \Lambda_{j,\alpha\beta\gamma}^k m_k^*\right)\right) + O(\Delta t^4) \quad \text{(B43)}$$

For $j = 0$, the equation becomes:

$$\partial_t m_0 + \partial_\alpha \underbrace{m_\alpha^*}_{=m_\alpha^{eq} + \frac{\Delta t}{2} f_\alpha} - \frac{\Delta t}{2}\left(\underbrace{\partial_t^2 m_0 - \partial_{\alpha\beta}(m_{\alpha\beta}^* + c_s^2 m_0^* \delta_{\alpha\beta})}_{(1)}\right) - \frac{\Delta t^2}{6}\left(\underbrace{\partial_t^3 m_0 + \partial_{\alpha\beta\gamma}\left(m_{\alpha\beta\gamma}^* + c_s^2(m_\alpha^*\delta_{\beta\gamma} + m_\beta^*\delta_{\alpha\gamma} + m_\gamma^*\delta_{\alpha\beta})\right)}_{(2)}\right) = O(\Delta t^3) \quad \text{(B44)}$$

(1) can then be detailed by expanding $\partial_t^2 m_0$ using Eq(B32) and $m_{\alpha\beta}^*$ using (B27)

$$(1) = -\partial_\alpha \left[\partial_t \left(m_\alpha + \frac{\Delta t}{2} f_\alpha\right) + \partial_\beta \left(m_{\alpha\beta}^{eq} + m_0^{eq} c_s^2 \delta_{\alpha\beta} + (\tau_{\alpha\beta} - 1/2)\, S_{\alpha\beta} - \Delta t\,(\tau_{\alpha\beta} - 1)\,\Pi_{\alpha\beta}^{eq}\right)\right] + O(\Delta t^2) \quad \text{(B45)}$$

Which gives (using Eq(B39)):

$$(1) = -\partial_\alpha \left(F_\alpha + \partial_\beta \frac{\Delta t}{2} \Pi_{\alpha\beta}^{eq}\right) + O(\Delta t^2) \quad \text{(B46)}$$

In (2), $\partial_t^3 m_0$ can be developed by using Eq(B19) and Eq(B25) successively, which gives:

$$(2) = \partial_\alpha \left[\partial_\beta \left(\partial_t \left(m_{\alpha\beta}^* + m_0^* c_s^2 \delta_{\alpha\beta}\right) + \partial_\gamma \left(m_{\alpha\beta\gamma}^* + c_s^2 \left(m_\alpha^* \delta_{\beta\gamma} + m_\beta^* \delta_{\alpha\gamma} + m_\gamma^* \delta_{\alpha\beta}\right)\right)\right) - \partial_t F_\alpha\right] + O(\Delta t) \quad \text{(B47)}$$

Which can be reduced to:

$$(2) = \partial_\alpha \left(\partial_\beta \Pi_{\alpha\beta}^{eq} - \partial_t F_\alpha\right) + O(\Delta t) \quad \text{(B48)}$$

By combining the expression of (1) and (2), the equation that is solved by the first moment of the main population is finally given by:

$$\partial_t m_0 + \partial_\alpha m_\alpha^{eq} = \Delta t^2 \partial_\alpha \left(\frac{1}{12} \partial_\beta \Pi_{\alpha\beta}^{eq} - \frac{1}{6} \partial_t F_\alpha \right) + O(\Delta t)^3 \tag{B49}$$

Finally, for $j = \alpha$, Eq(B43) comes as:

$$\begin{aligned} &\partial_t m_\alpha + \partial_\beta \left(m_{\alpha\beta}^* + m_0^* c_s^2 \delta_{\alpha\beta} \right) + \\ &\qquad \frac{\Delta t}{2} \left(\underbrace{\partial_t^2 m_\alpha - \partial_{\beta\gamma} \left(m_{\alpha\beta\gamma}^* + c_s^2 \left(m_\alpha^* \delta_{\beta\gamma} + m_\beta^* \delta_{\alpha\gamma} + m_\gamma^* \delta_{\alpha\beta} \right) \right)}_{(1)} \right) + \\ &\qquad\qquad \frac{\Delta t^2}{6} \left(\underbrace{\partial_t^3 m_\alpha + \partial_{\beta\gamma\mu} \sum_k \Lambda_{\alpha,\beta\gamma\mu}^k m_k^*}_{(2)} \right) + O(\Delta t^3) \end{aligned} \tag{B50}$$

$\sum_k \Lambda_{\alpha,\beta\gamma\mu}^k m_k^*$, can actually be expressed but was simply to long to be inserted in the same expression as the rest. It is given by:

$$\begin{aligned} &\sum_k \Lambda_{\alpha,\beta\gamma\mu}^k m_k^* = \\ &\qquad m_{\alpha\beta\gamma\mu}^* + c_s^2 (m_{\alpha\beta}^* \delta_{\gamma\mu} + m_{\alpha\gamma}^* \delta_{\beta\mu} + m_{\alpha\mu}^* \delta_{\beta\gamma} + m_{\beta\gamma}^* \delta_{\alpha\mu} + m_{\beta\mu}^* \delta_{\alpha\gamma} + m_{\gamma\mu}^* \delta_{\alpha\beta}) + \\ &\qquad\qquad m_0^* c_s^4 (\delta_{\alpha\beta}\delta_{\gamma\mu} + \delta_{\alpha\gamma}\delta_{\beta\mu} + \delta_{\alpha\mu}\delta_{\beta\gamma}) \end{aligned} \tag{B51}$$

To express (2), $\partial_t^3 m_\alpha$ must be expanded by using Eq. (B19)*, then Eq.* (B25) *and finally the definition of $\Pi_{\alpha\beta}$:*

$$\begin{aligned} \partial_t^3 m_\alpha &= \partial_t^2 F_\alpha - \partial_\beta \partial_t^2 \left(m_{\alpha\beta}^* + m_0 c_s^2 \delta_{\alpha\beta} \right) + \partial_t \partial_{\beta\gamma} \left[\sum_k \left(\Lambda_{\alpha\beta,\gamma}^k m_k^* - \Lambda_{\alpha\beta,\gamma}^k m_k^* \right) \right] + O(\Delta t) \\ &= \partial_t^2 F_\alpha - \partial_\beta \partial_t \Pi_{\alpha\beta} + \partial_{\beta\gamma} \partial_t \left(m_{\alpha\beta\gamma^*} + \left[m_\gamma^* \delta_{\alpha\beta} + m_\alpha \delta_{\beta\gamma} + m_\beta^* \delta_{\alpha\gamma} \right] c_s^2 \right) + O(\Delta t) \end{aligned} \tag{B52}$$

By underlining that:

$$\begin{aligned} \sum_k \left(\Lambda_{\alpha,\beta\gamma\mu}^k m_k^* \right) = \sum_k \left(\Lambda_{\alpha\beta\gamma,\mu}^k m_k^* \right) + \left[m_{\alpha\mu}^* \delta_{\beta\gamma} + m_{\beta\mu}^* \delta_{\alpha\gamma} + m_{\gamma\mu}^* \delta_{\alpha\beta} \right] c_s^2 + \\ m_0^* \left[\delta_{\alpha\beta}\delta_{\gamma\mu} + \delta_{\alpha\gamma}\delta_{\beta\mu} + \delta_{\alpha\mu}\delta_{\beta\gamma} \right] c_s^4 \end{aligned} \tag{B53}$$

and that according to Eq. (B25)*:*

$$\partial_t m_\alpha + \partial_\beta (m_{\alpha\beta} + m_0 c_s^2 \delta_{\alpha\beta}) = F_\alpha + O(\Delta t) \tag{B54}$$

(2) can be expressed as a composition of $\Pi^{eq}_{\alpha\beta\gamma}$ and $\Pi^{eq}_{\alpha\beta}$:

$$(2) = \left[\partial_t^2 F_\alpha + c_s^2 \partial_{\beta\gamma} \left(F_\alpha \delta_{\beta\gamma} + F_\beta \delta_{\alpha\gamma} + F_\gamma \delta_{\alpha\beta}\right)\right] + \partial_{\beta\gamma} \Pi^{eq}_{\alpha\beta\gamma} - \partial_\beta \partial_t \Pi^{eq}_{\alpha\beta} + O(\Delta t) \tag{B55}$$

Developing $\partial_t^2 m_\alpha$ using Eq. (B39), and developing $m_{\alpha\beta\gamma}$ using Eq. (B42), (1) is expressed as:

$$(1) = \partial_t F_\alpha - \partial_\beta \left(\Pi_{\alpha\beta} + \Delta t \left[\left(\tau_{\alpha\beta} - 1/2\right) \partial_t \Pi^{eq}_{\alpha\beta} + \left(\tau_{\alpha\beta\gamma} - 1\right) \partial_\gamma \Pi^{eq}_{\alpha\beta\gamma}\right]\right) \tag{B56}$$

By combining the expressions of (1), (2) and $m^*_{\alpha\beta}$ (Obtained through Eq(B42), the 2nd order equivalent equation to the algorithm comes as follow:

$$\begin{aligned}
&\partial_t \left(m_\alpha + \frac{\Delta t}{2} F_\alpha\right) + \partial_\beta \left(m_{\alpha\beta} + m_0^{eq} c_s^2 \delta_{\alpha\beta} + \left(\tau_{\alpha\beta} - 1/2\right) S_{\alpha\beta}\right) \\
&\qquad = \Delta t(\tau_{\alpha\beta} - 1/2)\Pi^{eq}_{\alpha\beta} + F_\alpha \\
&+ \Delta t^2 \partial_\beta \left[\left(\left[\tau_{\alpha\beta} - \frac{1}{2}\right]^2 - \frac{1}{6}\right) \partial_t \Pi^{eq}_{\alpha\beta} + \left(\left[\tau_{\alpha\beta\gamma} - \frac{1}{2}\right]\left[\tau_{\alpha\beta} - \frac{1}{2}\right] - \frac{1}{12}\right) \partial_\gamma \Pi^{eq}_{\alpha\beta\gamma}\right] \\
&\qquad - \frac{\Delta t^2}{6} \left[\partial_t^2 F_\alpha + c_s^2 \partial_{\beta\gamma} \left(F_\alpha \delta_{\beta\gamma} + F_\beta \delta_{\alpha\gamma} + F_\gamma \delta_{\alpha\beta}\right)\right] + O(\Delta t^3)
\end{aligned} \tag{B57}$$

Appendix C: Macroscopic equation

The conservation equation for momentum to the order 2 is given by Eq .(B39). By expressing the moments of the equilibrium function, it comes as:

$$\partial_t \rho u_\alpha + \partial_\beta \left(\rho u_\alpha u_\beta + p \delta_{\alpha\beta} + p^\sigma_{\alpha\beta}\right) = \Delta t(\tau_{\alpha\beta} - 1/2)\partial_\beta \Pi^{eq}_{\alpha\beta} \tag{C1}$$

Noting that in the previous expression, for the sake of clarity no volumic force are considered. This equation can be extended by determining the expression of $\Pi^{eq}_{\alpha\beta}$. This calculation is given for $\alpha = x$, the method being symmetrical for x and y direction the equation obtained for $y - direction$ is similar. $\partial_\beta \Pi^j_{x\beta}$ is given by:

$$\partial_\beta(\tau_{x\beta} - 1/2)\Pi^{eq}_{x\beta} = \left(\tau_\nu - 1/2\right)\left(\partial_x \Pi^{eq}_\nu + \partial_y \Pi^{eq}_{xy}\right) + \partial_x(\tau_b - 1/2)\Pi^{eq}_b \tag{C2}$$

With

$$\Pi^{eq}_\nu = \partial_t \sum_i H_{\nu,i} f_i^{eq} + \partial_\gamma \sum_i H_{\nu,i} \xi_{\gamma,i} f_i^{eq} \tag{C3}$$

$$\Pi^{eq}_{xy} = \partial_t \sum_i H_{xy,i} f_i^{eq} + \partial_\gamma \sum_i H_{xy,i} \xi_{\gamma,i} f_i^{eq} \tag{C4}$$

$$\Pi_b^{eq} = \partial_t \sum_i H_{b,i} f_i^{eq} + \partial_\gamma \sum_i H_{b,i} \xi_{\gamma,i} f_i^{eq} \tag{C5}$$

Giving that

$$H_{b,i}\xi_{\gamma,i} = \frac{H_{xx\gamma,i} + H_{yy\gamma,i}}{2} + c_s^2 H_{\gamma,i} \tag{C6}$$

$$H_{\nu,i}\xi_{\gamma,i} = \frac{H_{xx\gamma,i} - H_{yy\gamma,i}}{2} + c_s^2 H_{x,i}\delta_{\gamma x} - c_s^2 H_{y,i}\delta_{\gamma y} \tag{C7}$$

$$H_{xy,i}\xi_{\gamma,i} = H_{xy\gamma,i} + c_s^2 \left(H_{x,i}\delta_{\gamma y} + H_{y,i}\delta_{\gamma x}\right) \tag{C8}$$

By integrating the definition of the equilibrium function Eq. (31), it gives:

$$\Pi_\nu^{eq} = \partial_t \left(\frac{\rho u_x^2 - \rho u_y^2}{2}\right) + \partial_x \left(\frac{(p - \rho c_s^2)u_x}{2} + \rho c_s^2 u_x\right) + \partial_y \left(\frac{(p - \rho c_s^2)u_y}{2} + \rho c_s^2 u_y\right) \tag{C9}$$

$$\Pi_b^{eq} = \partial_t \left(\frac{\rho u_x^2 + \rho u_y^2}{2} + (p - \rho c_s^2)\right) - \partial_x \left(\frac{(p - \rho c_s^2)u_x}{2} - \rho c_s^2 u_x\right) + \partial_y \left(\frac{(p - \rho c_s^2)u_y}{2} - \rho c_s^2 u_y\right) \tag{C10}$$

$$\Pi_{xy}^{eq} = \partial_t \rho u_x u_y + \partial_x \left((p - \rho c_s^2)u_y + \rho c_s^2 u_y\right) + \partial_y \left((p - \rho c_s^2)u_x + \rho c_s^2 u_x\right) \tag{C11}$$

By merging Eqs. (C9, C10, C11) into Eq. (C2), the macroscopic equation that is solved by the scheme is:

$$\begin{aligned} &\partial_t \rho u_\alpha + \partial_\beta \left(\rho u_\alpha u_\beta + p\delta_{\alpha\beta} + p^\sigma_{\alpha\beta}\right) = \\ &\qquad \Delta t \partial_\beta \left(O(Ma^3) + (\tau_\nu - 1/2)p\left(\partial_\beta u_\alpha + \partial_\alpha u_\beta\right) + (\tau_b - \tau_\nu)p\partial_\gamma u_\gamma + Er_\alpha \delta_{\alpha\beta}\right) \end{aligned} \tag{C12}$$

where the error term reads

$$\begin{aligned} Er_\alpha = &-(\tau_\nu - 1/2)3\partial_\alpha \left((p - \rho c_s^2)u_\alpha\right) + \frac{3}{2}\left(\tau_\nu - \tau_b\right)\partial_\gamma \left((p - \rho c_s^2)u_\gamma\right) \\ &+ (\tau_b - 1/2)\left(\partial_t (p - \rho c_s^2) + \partial_\gamma \left((p - \rho c_s^2)u_\gamma\right)\right) \end{aligned} \tag{C13}$$

and the term $O(Ma^3)$ is an error proportional to the Mach number[66].

Appendix D: Recoloration

In this section, the equivalent macroscopic equation of the g_i population is determined. First of all, some value must be defined. The moments of the g_i population are noted:

$$m_j^{(g)} = \sum_i M_{ji} g_i \tag{D1}$$

By definition of ϕ $m_0^{(g)} = \rho\phi$. As previously, the algorithm that is followed by the phase field population function should be slightly re-formulated. The recoloration is expressed in the moment space:

$$m_j^{(g),*} = \phi m_j^* + S_j^{(3)} \tag{D2}$$

$$g_i(x, t + \Delta t) = g_i^*(x - \xi_{\alpha,i}, t) \tag{D3}$$

By expanding the streaming relationship:

$$g_i + \Delta t \partial_t g_i + \frac{\Delta t^2}{2} \partial_t^2 g_i = g_i^* + \Delta t \partial_t g_i^* + \frac{\Delta t^2}{2} g_i^* + O(\Delta t^3) \tag{D4}$$

Integrated into the moment space and by integrating Eq(B27) the last expression can be expressed:

$$m_j^{(g)} = m_j^{(g),*} + O(\Delta t) = \phi \left(m_j^{eq} + (\tau_j - 1/2) S_j \right) + S_j^{(3)} + O(\Delta t) \tag{D5}$$

Eq(D4) can be expressed at a higher degree:

$$m_j^{(g)} - m_j^{(g),*} = -\Delta t \left(\partial_t m_j^{(g)} + \partial_\alpha \sum_k \Lambda_{j,\alpha}^k m_k^{(g),*} \right) + O(\Delta t^2) \tag{D6}$$

For $j = 0$, giving that $m_0^{(g)} = m_0^{(g),*} = \rho\phi$ previous equation becomes:

$$\partial_t m_0^{(g)} + \partial_\alpha \left(\phi(m_\alpha^{eq}) + (\tau_\alpha - 1/2) S_\alpha \right) + S_\alpha^{(3)} \big) + O(\Delta t) \tag{D7}$$

Noting that $S_\alpha = \Delta t f_\alpha = O(\Delta t)$, $S_\alpha^{(3)} = O(\Delta t)$ and using the values of m_α^{eq} and $m_0^{(g)}$ it comes:

$$\partial_t \rho\phi + \partial_\alpha \rho\phi u_\alpha = O(\Delta t) \tag{D8}$$

Now Eq(D4) can be integrated into the moment space at its higher degree:

$$m_j^{(g)} - m_j^{(g),*} = -\Delta t \left(\partial_t m_j^{(g)} + \partial_\alpha \sum_k \Lambda_{j,\alpha}^k m_k^{(g),*} \right) - \frac{\Delta t}{2} \left(\partial_t^2 m_j^{(g)} - \partial_{\alpha\beta} \sum_k \Lambda_{j,\alpha\beta}^k m_k^{(g),*} \right) + O(\Delta t^2) \tag{D9}$$

To express this equation for $j = 0$, $\partial_t^2 m_0^{(g)}$ must be expanded:

$$\begin{aligned}\partial_t^2 m_j^{(g)} &= -\partial_t \partial_\alpha \phi m_\alpha^{eq} + O(\Delta t) = -\partial_\alpha \left(u_\alpha \partial_t \rho\phi + \phi\rho\partial_t u_\alpha\right) + O(\Delta t) \\ &= \partial_\alpha \left(u_\alpha \partial_\beta \left(\rho\phi u_\beta\right) + \rho\phi u_\beta \partial_\beta u_\alpha + \phi\partial_\beta p\delta_{\alpha\beta}\right) + O(\Delta t) \\ &= \partial_{\alpha\beta}\rho\phi u_\alpha u_\beta + \partial_\alpha\left(\phi\partial_\alpha p\right) + O(\Delta t) \end{aligned} \tag{D10}$$

To express the Δt^2, the spatial derivative must also be expressed:

$$\partial_{\alpha\beta}\sum_k \Lambda^k_{j,\alpha\beta} m_k^{(g),*} = m_{\alpha\beta}^{(g),*} + c_s^2 m_0^{(g),*}\delta_{\alpha\beta} = \partial_{\alpha\beta}(\rho\phi u_\alpha u_\beta + \phi p) + O(\Delta t) \tag{D11}$$

Finally, the final equation is given by:

$$\partial_t \rho\phi + \partial_\alpha \rho\phi u_\alpha = \partial_\alpha \left[\frac{p\Delta t}{2}\partial_\alpha \phi - S_\alpha^{(3)}\right] + O(\Delta t^2) \tag{D12}$$

This justifies the form of the collision term in the re coloration phase, to mimic the right term of the Allen-Cahn equation proposed by Chiu and Lin[43], the source term first moments must be:

$$S_\alpha^{(3)} = \frac{p\Delta t}{2}\frac{(1-\phi^2)}{W}\frac{\partial_\alpha \phi}{|\vec{\nabla}\phi|} \tag{D13}$$

This justifies the form of the source term proposed in this work. The moment of the source term is projected in the Hermite's polynomial base:

$$\Omega_i^{(3)} = w_i \frac{S_\alpha^{(3)} H_{\alpha,i}}{c_s^2} \tag{D14}$$

Which allows to recover Eq. (48). It is interesting to note that this operator is almost similar to the one originally proposed by D'Ortona[84] in 1995 and Latva-Kokko[72] in 2005. At the time, recoloration operator wasn't understood as a scheme allowing to solve a diffusion-advection equation for the phase field, and Chiu and Lin[43] only proposed their conservative form of the Allen-Cahn equation in 2011.

DATA AVAILABILITY

The data that support the findings of this study are available from the corresponding author upon reasonable request.

REFERENCES

[1]A. H. Lefebvre and V. G. Mcdonell, *CRC Press, Taylor and Francis* (CRC Press, 2017) p. 300.

[2]N. Ashgriz, *Handbook of Atomization and Sprays*, 1st ed. (Springer US, 2011).

[3]C. Hirt and B. Nichols, "Volume of fluid (VOF) method for the dynamics of free boundaries ," J. Comput. Phys. **1**, 201–225 (1981).

[4]S. Osher and J. Sethian, "Front propagating with curvature dependent speed: algorithm based on Hamilton-Jacobi formulations," J. Comput. Phys. **1**, 12–49 (1988).

[5]J. Van Der Waals and J. translation: Rowlinson, "The thermodynamic theory of capillarity under the hypothesis of a continuous density variation," Journal of Statistical Physic **20**, 197–244 (1979).

[6]D. Korteweg, "Sur la forme que prennent les équations du mouvements des fluides si l'on tient compte des forces capillaires causées par des variations de densité considérables mais continues et sur la théorie de la capilarité dans l'hypothèse d'une variation continue de la densité," Archive Néerlandaise des Sciences Exactes et Naturelles **II**, 1–24 (1901).

[7]J. Cahn and J. Hilliard, "Free energy of a nonuniform system. i. interfacial free energy," The jourenal of chemical physics **28**, 830–833 (1957).

[8]M. Baer and J. Nunziato, "A two phase mixture theory for the deflagration-to-detonation transition (DDT) in reactive granular materials," Int. J. Multiphase Flow **12**, 861–889 (1986).

[9]R. Saurel and R. Abgrall, "A simple method for compressible multifluid flows," SIAM J. Sci. Comput. **21**, 1115–1145 (1999).

[10]A. K. Kapila, R. Menikoff, J. B. Bdzil, S. F. Son, and D. S. Stewart, "Two-phase modeling of deflagration-to-detonation transition in granular materials: Reduced equations," Physics of Fluids **13**, 3002–3024 (2001).

[11]Richard Saurel, F. Petitpas, and R. A. Berry, "Simple and efficient relaxation methods for interfaces separating compressible fluids, cavitating flows and shocks in multiphase mixtures," Journal of Computational Physics **228**, 1678–1712 (2009).

[12]F. Fraysse and R. Saurel, "Automatic differentiation using operator overloading (ADOO) for implicit resolution of hyperbolic single phase and two-phase flow models," Journal of Computational Physics **399**, 108942 (2019).

[13]D. M. Anderson, G. B. McFadden, and A. A. Wheeler, "Diffuse-interface methods in fluid mechanics," Annual Review of Fluid Mechanics **30**, 139–165 (1998).

[14]R. Saurel and C. Pantano, "Diffuse-Interface Capturing Methods for Compressible Two-Phase Flows," Annual Review of Fluid Mechanics **50**, 105–130 (2018).

[15]U. Frisch, B. Hasslacher, and Y. Pomeau, "Lattice-Gas Automata for the Navier-Stokes Equation," Physical Review Letters **56**, 1505–1508 (1986).

[16]D. D'humières and P. Lallemand, "Lattice gas automata for fluid mechanics," Physica A: Statistical Mechanics and its Applications **140**, 326–335 (1986).

[17]G. McNamara and G. Zanetti, "Use of the Boltzmann Equation to Simulate Lattice-Gas Automata," Physical Review Letters **61**, 2332–2335 (1988).

[18]D. Rothman and J. Keller, "Immiscible Cellular-Automaton Fluids," Journal of Statistical Physics **52**, 1119–1127 (1988).

[19]A. Gustensen, D. Rothman, S. Zaleski, and G. Zanetti, "Lattice Boltzmann model of immiscible fluids," Physical Review A **43**, 4320–4327 (1988).

[20]W. Shao and J. Li, "Review of Lattice Boltzmann Method Applied to Computational Aeroacoustics," Archives of acoustics **44**, 215–238 (2019).

[21]Y. long Zhao and Z. ming Wang, "Multi-scale analysis on coal permeability using the lattice Boltzmann method," Journal of Petroleum Science and Engineering **174**, 1269–1278 (2019).

[22]T. Zhang and S. Sun, "A coupled Lattice Boltzmann approach to simulate gas flow and transport in shale reservoirs with dynamic sorption," Fuel **246**, 196–203 (2019).

[23]J. Wang, L. Chen, Q. Kang, and S. S. Rahman, "Apparent permeability prediction of organic shale with generalized lattice Boltzmann model considering surface diffusion effect," Fuel **181**, 478–490 (2016), arXiv:1601.00704.

[24]M. Tayyab, S. Zhao, and P. Boivin, "Lattice-Boltzmann modeling of a turbulent bluff-body stabilized flame," Physics of Fluids **33** (2021), 10.1063/5.0038089.

[25]M. Sakthivel and K. Anupindi, "An off-lattice Boltzmann method for blood flow simulation through a model irregular arterial stenosis: The effects of amplitude and frequency of the irregularity," Physics of Fluids **33** (2021), 10.1063/5.0044948.

[26]S. Saito, A. De Rosis, L. Fei, K. H. Luo, K. I. Ebihara, A. Kaneko, and Y. Abe, "Lattice Boltzmann modeling and simulation of forced-convection boiling on a cylinder," Physics of Fluids **33** (2021), 10.1063/5.0032743, arXiv:1912.02018.

[27]T. R. Mitchell, M. Majidi, M. H. Rahimian, and C. R. Leonardi, "Computational modeling of three-dimensional thermocapillary flow of recalcitrant bubbles using a coupled lattice Boltzmann-finite difference method," Physics of Fluids **33** (2021), 10.1063/5.0038171.

[28]Y. Li, J. Mu, C. Xiong, Z. Sun, and C. Jin, "Effect of visco-plastic and shear-thickening/thinning characteristics on non-Newtonian flow through a pipe bend," Physics of Fluids **33** (2021), 10.1063/5.0038366.

[29]A. De Rosis, J. Al-Adham, H. Al-Ali, and R. Meng, "Double-D2Q9 lattice Boltzmann models with extended equilibrium for two-dimensional magnetohydrodynamic flows," Physics of Fluids **33** (2021), 10.1063/5.0043998.

[30]K. J. Petersen and J. R. Brinkerhoff, "On the lattice Boltzmann method and its application to turbulent, multiphase flows of various fluids including cryogens: A review," Physics of Fluids **33** (2021), 10.1063/5.0046938.

[31]X. Shan and H. Chen, "Lattice boltzmann model for simulating flows with multiple phases and components," Physical Review E **47**, 1815–1820 (1993).

[32]X. Shan and H. Chen, "Simulation of non-ideal gases and liquid-gas phase transition by lattice boltzmann equation," Physical Review E **49**, 2941–2948 (1994).

[33]M. Swift, W. Osborn, and J. Yeomans, "Lattice boltzmann simulation of nonideal fluids," Physical Review Letters **75**, 830–833 (1995).

[34]M. Swift, E. Orlandini, W. Osborn, and J. Yeomans, "Lattice boltzmann simulations of liquid-gas and binary fluid systems," Physical Review E **54**, 5041–5052 (1996).

[35]X. He, S. Chen, and R. Zhang, "A lattice boltzmann scheme for incompressible multiphase flow and its application in simulation of rayleigh-taylor instability," Journal of Computational Physics **152**, 642–663 (1999).

[36]A. Fakhari and T. Lee, "Multiple-Relaxation-Time lattice Boltzmann method for immiscible fluids at high Reynold numbers," Physical Review E **87**, 023304 (2013).

[37]A. Fakhari, M. Geier, and T. Lee, "A mass-conserving lattice boltzmann method with dynamic grid refinement for immiscible two-phase flows," Journal of Computational Physics **315**, 434–457 (2016).

[38]A. Fakhari and D. Bolster, "Diffuse interface modeling of three-phase contact line dynamics on curved boundaries: A lattice Boltzmann model for large density and viscosity ratios," Journal of Computational Physics **334**, 620–638 (2017).

[39]A. Fakhari, T. Mitchell, C. Leonardi, and D. Bolster, "Improved locality of the phase-field lattice-Boltzmann model for immiscible fluids at high density ratios," Physical Review E **96**, 053301 (2017).

[40]M. Geier, A. Fakhari, and T. Lee, "A conservatice phase-field lattice boltzmann model for interface tracking equation," Physical Review E **91**, 063309 (2015).

[41]T. Mitchell, C. Leonardi, and A. Fakhari, "Development of a three-dimensional phase-field lattice boltzmann method for the study of immicible fluids at high density ratio," Int. J. multiphase flow **107**, 1–15 (2018).

[42]Y. Sun and C. Beckermann, "Sharp interface tracking using the phase-field equation," Journal of Computational Physics **220**, 626–653 (2007).

[43]P. Chiu and Y.-T. Lin, "A conservative phase field method for solving compressible two phase flows," Journal of computational Physics **230**, 185–204 (2011).

[44]M. Wöhrwag, C. Semprebon, Mazloomi, A. Moqaddam, I. Karlin, and H. Kusumaatmaja, "Ternary free-energy entropic lattice boltzmann model with a high density ratio," Physical review Letters **120**, 234501 (2018).

[45]S. Saito, A. De Rosis, A. Festuccia, A. Kaneko, Y. Abe, and K. Koyama, "Color-gradient lattice boltzmann model with monorthogonal central moments: hydrodynamic melt-jet breakup simulations," Physical Review E **98**, 013305–2948 (2018).

[46]Y. Yu, H. Liu, D. Liang, and Y. Zhang, "A versatile lattice Boltzmann model for immiscible ternary fluid flows," Physics of Fluids **31** (2019), 10.1063/1.5056765, arXiv:1808.08555.

[47]T. Inamuro, T. Echizen, and F. Horai, "Validation of an improved lattice Boltzmann method for incompressible two-phase flows," Computers and Fluids **175**, 83–90 (2018).

[48]S. Mukherjee, P. Berghout, and H. E. Van den Akker, "A lattice boltzmann approach to surfactant-laden emulsions," AIChE Journal **65**, 811–828 (2019).

[49]M. Monteferrante, A. Montessori, S. Succi, D. Pisignano, and M. Lauricella, "Lattice Boltzmann multicomponent model for direct-writing printing," Physics of Fluids **33** (2021), 10.1063/5.0046555.

[50]H. Liu, Q. Kang, C. Leonardi, S. Schmieshek, A. Narvaez, B. Jones, J. Williams, A. Valocchi, and J. Harting, "Multiphase lattice boltzmann simulations for porous media applications," Comput Geosci **20**, 777–805 (2016).

[51]R. Saurel, P. Boivin, and O. Le Métayer, "A general formulation for cavitating, boiling and evaporating flows," Computers & Fluids **128**, 53–64 (2016).

[52]D. W. Davis and B. Chehroudi, "Shear-coaxial jets from a rocket-like injector in a transverse acoustic field at high pressures," 44th AIAA Aerospace Sciences Meeting and Exhibit **13**, 9173–9190 (2006).

[53]F. Baillot, J. B. Blaisot, G. Boisdron, and C. Dumouchel, "Behaviour of an air-assisted jet submitted to a transverse high-frequency acoustic field," Journal of Fluid Mechanics **640**, 305–342 (2009).

[54]A. Qi, L. Y. Yeo, and J. R. Friend, "Interfacial destabilization and atomization driven by surface acoustic waves," Physics of Fluids **20** (2008), 10.1063/1.2953537.

[55]J. M. Apeloig, F. X. D'Herbigny, F. Simon, P. Gajan, M. Orain, and S. Roux, "Liquid-fuel behavior in an aeronautical injector submitted to thermoacoustic instabilities," Journal of Propulsion and Power **31**, 309–319 (2015).

[56]E. Lo Schiavo, D. Laera, E. Riber, L. Gicquel, and T. Poinsot, "Effects of liquid fuel/wall interaction on thermoacoustic instabilities in swirling spray flames," Combustion and Flame **219**, 86–101 (2020).

[57]T. Christou, B. Stelzner, and N. Zarzalis, "Influence of an oscillating airflow on the prefilming airblast atomization process," Atomization and Sprays **31**, 1–14 (2021).

[58]T. Reis and T. Phillips, "Lattice Boltzmann model for simulating immiscible two-phase flows," Journal of Physics A **40**, 4033–4053 (2007).

[59]H. Liu, A. Valocchi, and K. Q.J., "Three dimensionnal lattice boltzmann model for immiscible two phase flow simulations," Physical review E **85**, 046309 (2012).

[60]A. Subhedar, A. Reiter, M. Selzer, F. Varnik, and B. Nestler, "Interface tracking characteristics of color-gradient lattice boltzmann model for immiscible fluids," Physical Review E **101**, 013313 (2020).

[61]S. Leclaire, A. Parmigiani, B. Chopard, and J. Latt, "Three-dimensional lattice Boltzmann method benchmarks between color-gradient and pseudo-potential immiscible multi-component models," International Journal of Modern Physics C **28** (2017), 10.1142/S0129183117500851.

[62]D. Gueyffier, J. Li, R. Scardovelli, and S. Zaleski, "Volume-of-Fluid interface tracking with smoothed surface stress methods for three-dimensional flows," Journal of Computational Physics **152**, 423–456 (1998).

[63]G. Périgaud and R. Saurel, "A compressible flow model with capillary effectd," Journal of computational physics **209**, 139–178 (2005).

[64]Y. Ba, H. Liu, Q. Li, Q. Kang, and J. Sun, "Multiple-relaxation-time color-gradient lattice Boltzmann model for simulating two-phase flows with high density ratio," Physical Review E **94**, 1–15 (2016).

[65]J. Brackbill, D. Kothe, and C. Zemach, "A continuum method for modeling surface tension," Journal of Computation Physics **100**, 335–354 (1992).

[66]T. Krüger, A. Kusumaatmaja, A. Kuzmin, O. Shardt, G. Silva, and E. Viggen, *The Lattice Boltzmann Method, Principles and Practice*, 1st ed. (Springer Nature, 2017).

[67]S. Leclaire, M. Reggio, and J. Trépanier, "Isotropic color gradient for simulating very high-density ratios with a two-phase flow lattice Boltzmann model," Computers and fluids **48**, 98–112 (2011).

[68]D. Grunau, S. Chen, and K. Eggert, "A lattice Boltzman model for multiphase fluid flows," Physics of fluids A **5**, 2557–2562 (1993).

[69]O. L. Métayer, J. Massoni, and R. Saurel, "Élaboration des lois d ' état d ' un liquide et de sa vapeur pour les modèles d ' écoulements diphasiques Elaborating equations of state of a liquid and its vapor for two-phase flow models," International journal of thermal sciences **43**, 265–276 (2004).

[70]P. Boivin, M. Cannac, and O. Le Métayer, "A thermodynamic closure for the simulation of multiphase reactive flows," International Journal of Thermal Sciences **137**, 640–649 (2019).

[71]A. Chiapolino, P. Boivin, and R. Saurel, "A simple and fast phase transition relaxation solver for compressible multicomponent two-phase flows," Computers and Fluids **150**, 31–45 (2017).

[72]M. Latva-Kokko and D. Rothman, "Diffusion properties of gradient-based lattice Boltzmann models of immiscible fluids," Physical review E **71**, 056702 (2005).

[73]S. Leclaire, N. Pellerin, M. Reggio, and J.-Y. Trépanier, "Enhanced equilibrium distribution functions for simulating immiscible multiphase flows with variable density ratios in a class of lattice boltzmann models," International Journal of Multiphase Flow **57**, 159–168 (2013).

[74]S. Leclaire, N. Pellerin, M. Reggio, and J.-Y. Trépanier, "Unsteady immiscible multiphase flow validation of a multiplerelaxation-time lattice boltzmann method," Journal of Physics A: Mathematical and Theoretical **47**, 105501 (2014).

[75]S. Leclaire, A. Parmigiani, O. Malaspinas, C. B., and L. J., "Generalized three-dimensional lattice boltzmann color-gradient method for immiscible two-phase pore-scale imbition and drainage in porous media," Physical Review E **95**, 033306 (2017).

[76]P. Bhatnagar, E. Gross, and M. Krook, "A Model for Collision Processes in Gases. I. Small Amplitude Processes in Charged and Neutral One-Component Systems," Physical Review **94**, 511–525 (1954).

[77]G. Farag, S. Zhao, G. Chiavassa, and P. Boivin, "Consistency study of lattice-boltzmann schemes macroscopic limit," Physics of Fluids **33**, 031701 (2021).

[78]Z. Wen, Q. Li, Y. Yu, and K. Luo, "Improved three-dimensional color-gradient lattice Boltzmann model for immiscible two-phase flows," Physical Review E **100**, 023301 (2019).

[79]Q. Li, K. Luo, Y. He, Y. Gao, and W. Tao, "Coupling lattice Boltzmann model for simulation of thermal flows on standard lattices," Physical Review E **85**, 016710 (2012).

[80]C. Pooley and K. Furtado, "Eliminating spurious velocities in the free-energy lattice boltzmann method," Physical Review E **77**, 046702 (2008).

[81]C. Semprebon, T. Krüger, and H. Kusumaatmaja, "Ternary free-energy lattice boltzmann model with tunable surface tensions and contact angles," Physical Review E **93**, 033305 (2016).

[82]O. Malaspinas, "Increasing stability and accuracy of the lattice Boltzmann scheme: recursivity and regularisation," arXiv , 1–31 (2015).

[83]F. Renard, Y. Feng, J. Boussuge, and P. Sagaut, "Improved compressible hybrid lattice boltzmann method on standard lattice for subsonic and supersonic flows," arXiv preprint arXiv:2002.03644 (2020).

[84]U. D'Ortona, D. Salin, M. Cieplak, R. Rybka, and J. Banavar, "Two-color nonlinear boltzmann cellular automate: Surface tension and wetting," Physical Review E **51**, 3718–3728 (1995).

[85]I. Halliday, A. Hollis, and C. Care, "Lattice boltzmann algorithm for continuum multicomponent flow," Physical review E **76**, 026708 (2007).

[86]S. Guo, Y. Feng, and P. Sagaut, "Improved standard thermal lattice boltzmann model with hybrid recursive regularization for compressible laminar and turbulent flows," Physics of Fluids **32**, 126108 (2020).

[87]F. Dubois, "Equivalent partial differential equations of a lattice Boltzmann scheme," Computers and Mathematics with Applications **55**, 1441–1449 (2008).

[88]K. Burgin, J. Spendlove, X. Xu, and I. Halliday, "Kinematics of chromodynamic multicomponent lattice Boltzmann simulation with a large density contrast," Physical Review E **100**, 1–15 (2019).

[89]A. S. Suiker and C. S. Chang, "Application of higher-order tensor theory for formulating enhanced continuum models," Acta Mechanica **142**, 223–234 (2000).

[90]S. Wolfram, "Cellular automaton fluids 1: Basic theory," Journal of Statistical Physics **45**, 471–526 (1986).

[91]D. Holdych, D. Rovas, J. Georgiadis, and R. Buckius, "An improved hydrodynamics formulation for multiphase flow lattice-boltzmann models," International Journal of Modern Physics C **9**, 1393–1404 (1998).

[92]N. Che Sidik and T. Tanahashi, "Two-phase flow simulation with lattice boltzmann method," J. Mekanikal **24**, 68–79 (2007).

[93]H. Huang and X. Lu, "Relative permeabilities and coupling effects in steady-state gas-liquid flow in porous media: A lattice Boltzmann study," Physic of fluids **21**, 092104 (2009).

[94]L. Rayleigh, "On The Instability Of Jets," Proceedings of the London Mathematical Society **s1-10**, 4–13 (1878).

[95]X. He, X. Shan, and D. G.D., "Discrete boltzmann equation model for nonideal gases," Physical Review E **57**, R13–R16 (1998).

[96]Z. Guo, C. Zheng, and B. Shi, "Discrete lattice effects on the forcing term in the lattice boltzmann method," Physical Review E **65**, 046308 (2002).